Contents

Chapter 1

Chemical model diagnostics using graph theory and metrics.

"The complexities of cause and effect defy analysis."

- Douglas Adams, *Dirk Gently's Holistic Detective Agency*

1.1 Introduction

The node-link (ball-stick) [REF SECTION] style structure has long been used to represent real-world relationships between items. Such a structure is complementary to our cognitive disposition towards pattern recognition [citep]. It is for this reason that the node-link visualisation format has been used for anything ranging from transportation maps [citep BECK] to the differentiation of ancestorial lineages of the human race (Figure 1.1). However, the abundance and complexity of real-world data often present us with difficulties in manually representing it in a useful form. In SECTION XX it is suggested this may be overcome with the use of computational analysis and automated visualisation tools. Such methods usually require a level of data manipulation to transform the data into a machine parseable form.

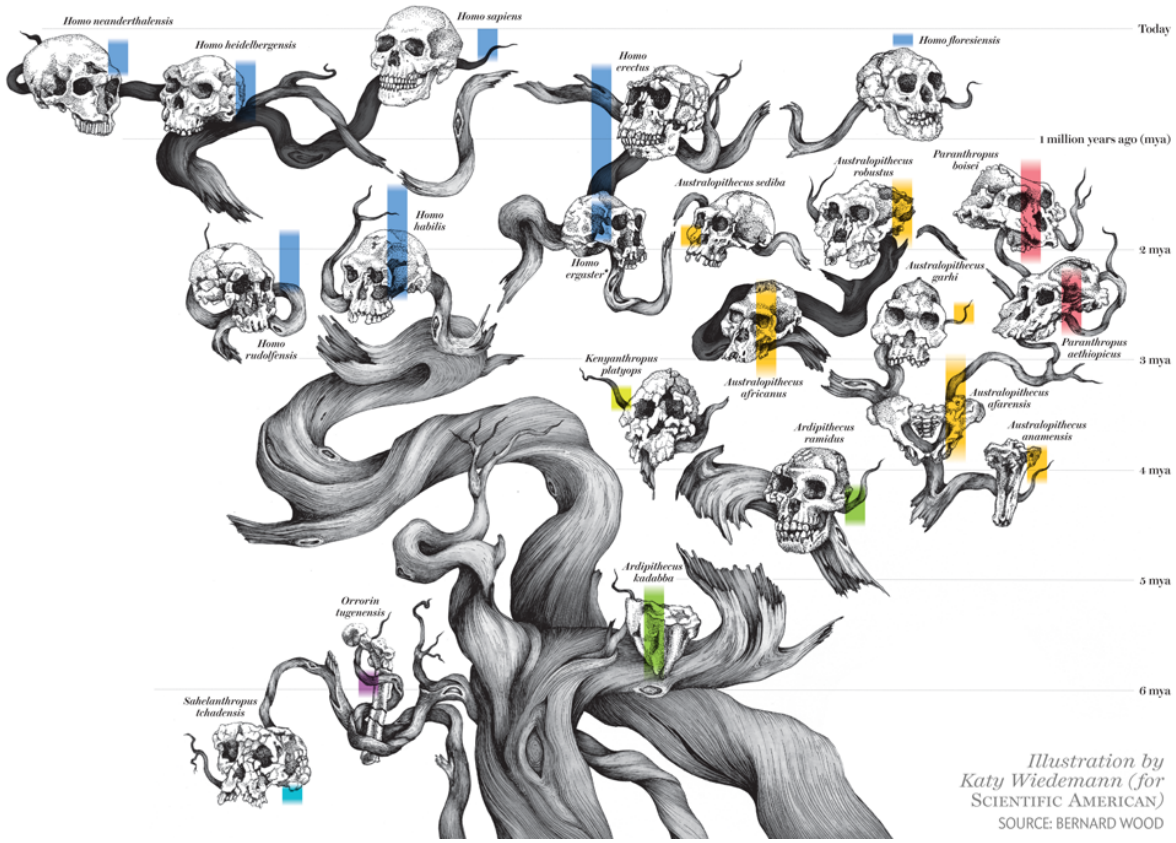

Figure 1.1: **The human family tree.** This is a visual depiction of the human lineage, starting with our common ancestorial roots. In SECTION it was shown that the use of trees / graphs[1]is useful in showing relationships between items. Source: [Wood, 2014]

In the field of mathematics a graph, $G(\nu, \epsilon, \omega)$, is defined as a function of items (vertices[2]), ν which are connected through a series of connections (or edges[1]) representing any relationships between them, ϵ.

[1]A tree is a special case of a graph

[2]The term node, item or vertex shall be used interchangeably for the remainder of this chapter. This also applies to links/relationships/edges and edge-weight/strength

Since relationships in the real world are rarely equivalent, we then encode the importance of each link in the form of an edge weight, or strength - ω. Such formats allow both numerical and computational algorithms to understand and interpret the graph structure, providing us with information about the data or make use of automated layout programs for visualisation.

This chapter builds on the work shown in SECTION XXX - where the ability to represent complex data in the form of a graph was used to (visually) draw information regarding network structure and temporal changes. Here I will begin by exploring situations where the visual representation of many, large or complex networks is impractical. We start by introducing a series of mathematical approaches which are capable of quantifying the graph (and nodes within it) and apply them to the co-author network for papers regarding the Master Chemical Mechanism, section 1.2. Following these global metrics are used to categorise the chemistry within different mechanism subsets, and provide us with an insight to the chemistry structure (SECT LABEL) and finally apply these to real-world simulations representing a range of environments (marine, rainforest and urban) in SECTREF.

This allows for a higher level of automated analysis which can be used to batch process, analyse and categorise chemical simulations. section 1.2 begins by introducing the most common of the graph metrics which can be used for analysis. To do this a citation graph is generated by web-scraping google scholar results.

1.2 Graph Metrics

An increase in the ability to gather and store data results in a difficulty to understand it (ref SECTION). The production of large, multivariate networks of inexplicable complexity greatly hinders our ability to draw out meaningful conclusions based on visualisation alone. This means that much like the generation of mechanism, or creating semi-automated graph drawing layouts, we must rely on the field of mathematics coupled with computational aid (REF SECTION).

Numerical algorithm, derived from the field of Graph Theory can be used to circumvent the need for individual graph analysis and provide us with information about the network. One such subset of numerical algorithms are regarded as "centrality metrics", and may be used to rank the role and importance (centrality) of a node. In the following sub-section, the most common (REF PAPER) centrality metrics are discussed and applied to the MCM citation network.

1.2.1 Centrality metrics and academic publishing.

One common application for graph analysis and visualisation is the representation and prediction of citation counts within academic journals [Small, 1973; Page et al., 1999; Monastersky and Van Noor-

den, 2019; Molontay and Nagy, 2020]. Here network-visualisation techniques may be used to highlight the origins of a paper - for instance, Figure 1.2 shows the multi-disciplinary research which underpins 6 prominent discoveries in the last 150 years.

To the properties presented by different centrality metrics (described above), we apply them to an approximate representation of the citation graph relating to the Master Chemical Mechanism (subsection 1.2.2).

1.2.2 The Master Chemical Mechanism (MCM)

The MCM, [**?**], is a near explicit representation of our foremost understanding of gas-phase tropospheric chemistry. The mechanism describes the oxidation of 143 primary emitted VOCs and the respective rates at which this occurs. It has been used in the...

Information on the chemistry, - x species - y ... first published and how this can be used with regards to the following algorithms are presented in REF JENKINS 15 ACP.

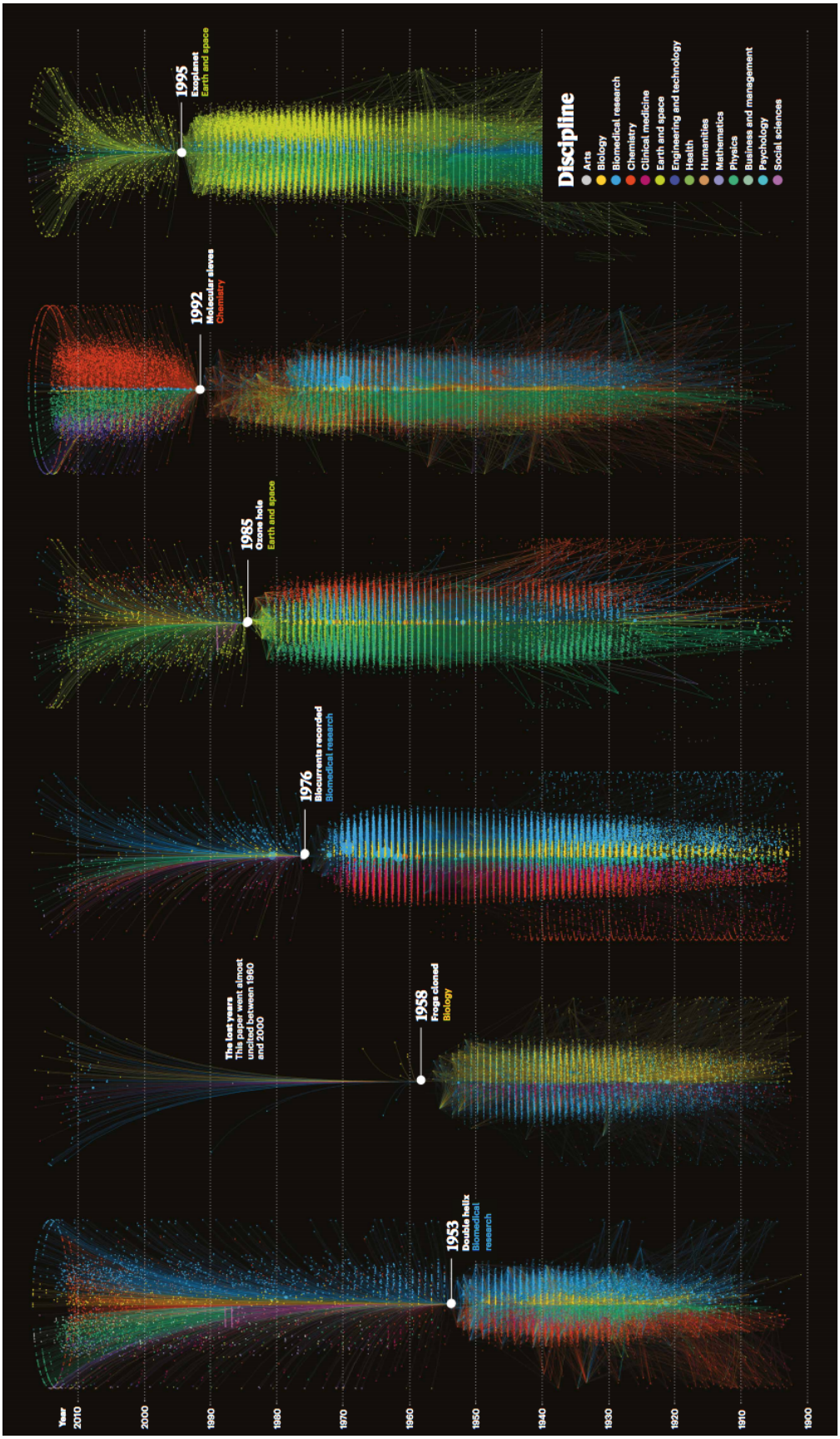

Figure 1.2: **150 years of letters to Nature.** A visualisation showing how previous research is used to inspire future studies. Important discoveries (DNA, Cloning(frogs), Bio-Currents, Ozone Hole, Molecular Sieves and Exoplanets) are split into research which contributed to their formation (below), and the consequent papers produced from each discovery. Use of colour is used to emphasise the multi-disciplinary nature of prolific scientific discovery. Source: [Barabási, 2019]

1.2.3 Data Collection

To generate a dataset on papers related to the MCM. The academic search engine (Google Scholar [Google, 2019]) is queried for all articles containing the words { *"Master", "Chemical", "Mechanism"* and *"MCM"* }. For each match, the first 100 pages of results are selected. Each of these contains 10 articles, from which the first 100 pages of related articles are chosen. In taking the top 1000 citations for each page a network of 15744 papers and 30178 citations[3] is created. This process made use of an edited version of the *etudier* Github repository, [Edsu and Ellis, 2019].

1.2.4 Visualising the data.

The initial visualisation of the dataset is accomplished through the use of THREE.js [Cabello, 2019]. This makes use of WebGL bindings and allows for the efficient viewing, querying and interacting of the data in 3 dimensions. This helped identify the temporal changes within the network by mapping a papers publication year to the z direction, Figure 1.3, as discussed in subsection 1.2.5.

[3]Note: this had the potential of returning up to 1000,000 nodes

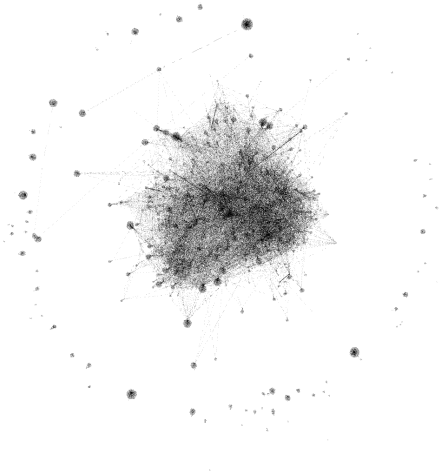

(a) A 2D force directed representation of the network using the gephi software [Bastian et al., 2009]

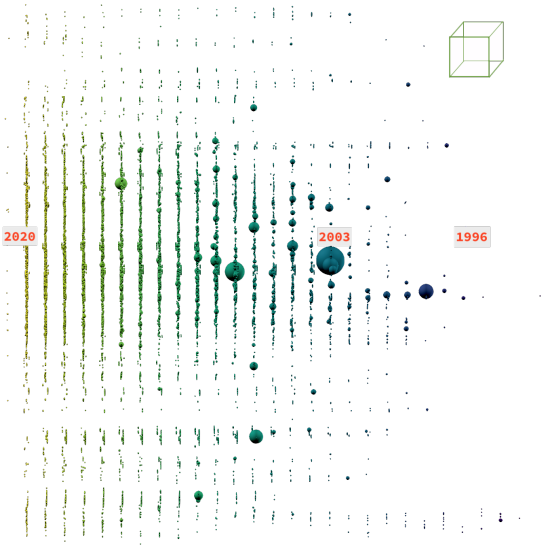

(b) 3D orthographic camera (sideview)

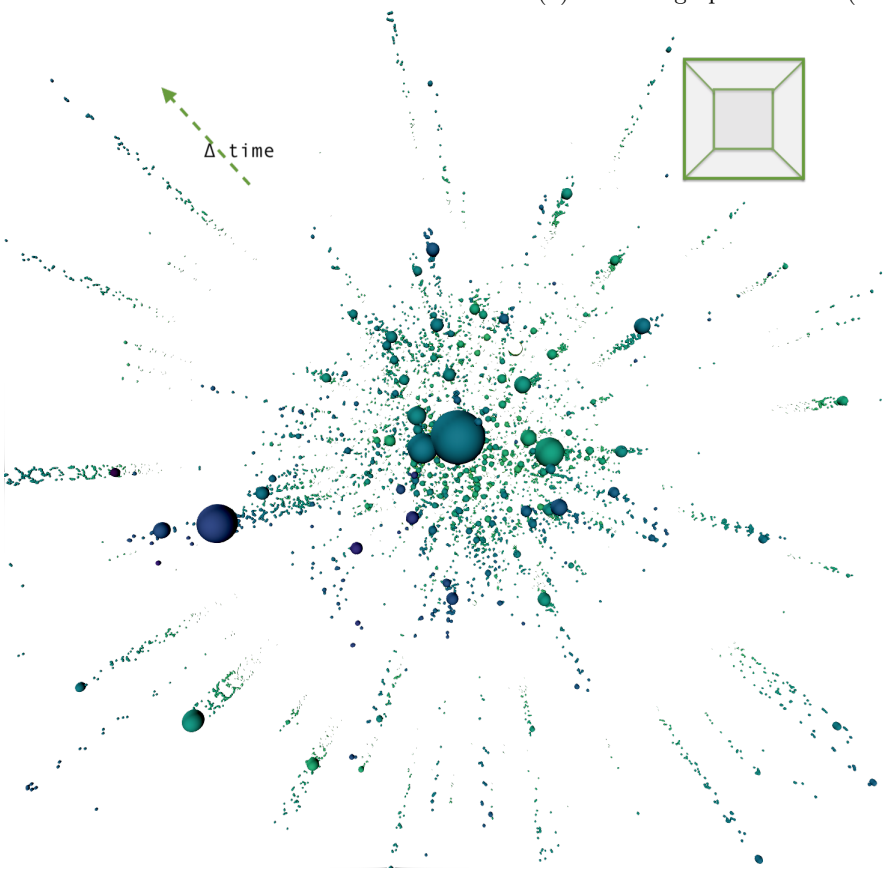

(c) 3D perspective camera

Figure 1.3: **Initial 3D graph representation of the scraped MCM citation graph.** (a) shows the 'classic' graph representation of the network. (b) shows a size representation using an orthographic perspective. Here time is shown across the x axis, with yellow being the most recent. (c) uses a perspective camera, which emphasizes the... Still captures of 2D and 3D visualisations of the dataset. Node size corresponds to the number of citations, and colour (and z-axis) corresponds to the publication year for each paper.

1.2.5 Filtering the data

In the method used to web scrape data, there are several features which need to be corrected/removed. The reasons for this are discussed below.

Pre-1996

There exist several papers predating the conception of the MCM (1996). A number of these can be attributed as incorrect data, with publication dates <1900 which may be the result of missing information or a fault in googles web scraping algorithm. Any such papers are removed from the dataset.

For otherwise correct articles, those published pre-1996 are also filtered from the dataset - this is because we are interested in identifying the influence the MCM has had on research and not the research that may have led to its creation. This can be seen in the cone-like shape emanating from the first MCM papers in Figure 1.3b.

N-th degree research

Not all research articles in a field reference other articles with the same field. Figure 1.2 showed us that many of the great discoveries in science have a multidisciplinary nature. It is for this reason that it is expected that articles from non-atmospheric areas of research may reference or build upon specific areas of research touched by the MCM. Such papers, and in consequence the papers which cite them, have little or no links to many of the core MCM papers. Such papers manifest themselves as a halo of satellite clusters which are connected by themselves but not with the main body of the graph, Figure 1.3a. In using a 3D perspective viewpoint (Figure 1.3c) it is possible to identify the paper which references the MCM and then the consequent papers which cite it by observing the satellite clusters, and the gradually lightening spiral of papers which emanate out of it.

Analysis of the network connections for each cluster can allow us to identify the indirect relationships some of these diverse topics (Table 1.1) contained within the satellite nodes. Here it can be seen that the use of photochemical ozone creation potentials [Derwent et al., 1998; Jenkin and Hayman, 1999] are used for the Life cycle assessment of Italian high-quality milk production [Fantin et al., 2012]. Similarly indirect paths such as the paper: "Temporal controls on dissolved organic matter and lignin biogeochemistry in a pristine tropical river" ([Spencer et al., 2010]) can be used to link to [Stubbins et al., 2008] and ultimately the MCM protocol paper [Saunders et al., 2003].

If we desired to remove such papers, the simplest method would be to recreate the graph into one

where links are drawn between papers that are cited together (subsection 1.2.6) and then removing any nodes without any external connections (isolates).

Fabrication of Bioinspired Actuated Nanostructures with Arbitrary Geometry and Stiffness	[Pokroy et al., 2009]
Temporal controls on dissolved organic matter and lignin biogeochemistry in a pristine tropical river	[Spencer et al., 2010]
Neuroproteomics in Neurotrauma	[Ottens et al., 2006]
Fast start-up of a pilot-scale deammonification sequencing batch reactor from an activated sludge inoculum	[Jeanningros et al., 2010]
Red blood cell oxidative stress impairs oxygen delivery and induces red blood cell aging	[Mohanty et al., 2014]
Life cycle assessment of Italian high quality milk production.	[Fantin et al., 2012]

Table 1.1: A selection of research papers not directly connected to the field of atmospheric modelling.

Unprobable occurances

Finally, the extracted network also contains many disconnected component subgraphs - graphs with no connection to atmospheric science. An example of this is seen in an article about neuroproteomics in neurotrauma [Ottens et al., 2006]. In analysing the paths which connect this, it is seen to cite the paper on "Large scale gene expression profiling of metabolic shift of mammalian cells in culture", [Korke et al., 2004]. This is an anomaly which within its structure contains the words "Master", "Chemical" and "Mechanism" (separately) and has ‘MCM’ as an abbreviation for one of the author names. To remove such papers, all disconnected sub-components are removed from the analysis.

A note on unintentional filtering

Author names and some extended titles may be truncated with the use of ellipses. This is due to the web scraping script extracting these directly from the Google scholar page, and not the original articles themselves. It is worth noting that the results in this section are not explicit, but rather a demonstration of graph theory on a real-world dataset.

1.2.6 The Co-citation Network

The document coupling techniques of co-citation was introduced in the 1970s as an alternative approach for quantifying the results within the science citation index [Small, 1973]. Rather than rep-

resenting a graph using backpropagation (through the use of referencing and citation counts), a co-citation network introduces a link between papers if, and only if, they have been cited together. Although this loses the directionality of a graph, it allows us to show forward propagating trends between papers within the same field.

Applying the above method allows us to reduce the citation graph of 451 papers and 5402 edges to an undirected co-citation graph of 2758 edges - halving the number of original links between papers.

1.2.7 The Co-authorship network

An alternative to exploring which papers which are cited together are to look at their authors. Here undirected links are drawn between authors on the same paper. This style of analysis was used to show that the number of papers per author, and the total number of authors per paper can vary between research fields, [Newman, 2004]. In combining this with a series of network centrality metrics, [Fujita et al., 2017] revealed that it is possible to discern promising researchers from both iter and Intra disciplinary groups.

In building a co-authorship network for the MCM, we can identify authors who publish together[4] and highlight research groups who work with the MCM, Figure 1.4. This shows how authors with a similar geographic location/institution are more likely to publish together. The largest cluster here falls under the MCM developer team, which resides between the Leeds and York universities. Next two German institutions which are heavily involved in the atmospheric chemistry field (Julrich and Max Planck), followed by an assortment of Chinese authors, mainly centred around the Beijing or Hong Kong region.

[4]Disclaimer: as mentioned earlier, not all authors for every paper were recorded by the web scraping algorithm

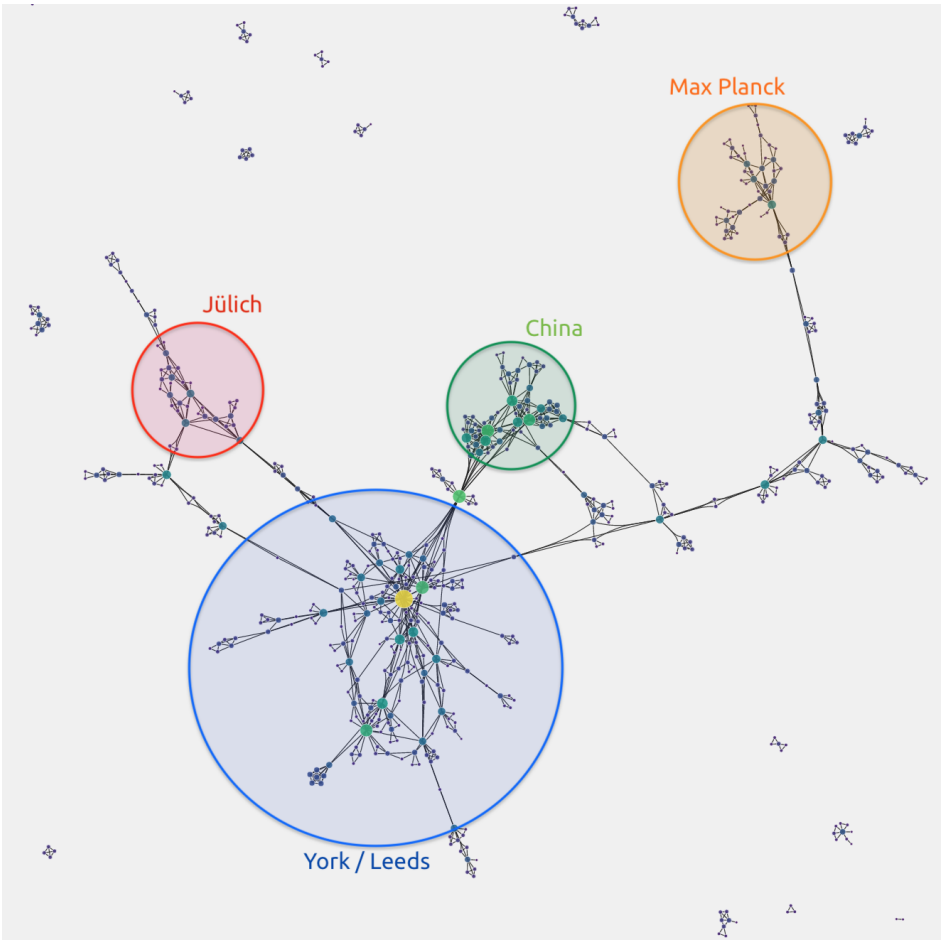

Figure 1.4: **The co-author network.** In representing the authorship network as a force directed graph we are able to see cliques or clusters of people who publish together. It can be noted that this often occurs when they have a similar geographical location.

1.3 Metric analysis

To demonstrate the information provided by different centrality metrics, a simple intuitive network (the co-author network in Figure 1.4) shall be used. This subsection will access the efficiency of graph centrality metrics in their ability to identify important nodes within a network.

1.3.1 Degree Centrality

The simplest, and most intuitive, metric is degree centrality [Freeman, 1978]. This is described as the sum of all links incident on a node - simply put, we count the number of edges going in and out of a node. This gives us an idea of the importance of a node and has been used to calculate influence within social media or the probability of a profile committing online auction fraud [Gemma, 2019; Freeman, 1978].

For the author network, Figure 1.5 we see that many of the names on the list are either contributors

to the MCM or have worked with them at Leeds. It is also seen that the authors with the most collaborations, or links, are very likely to appear within the most cited or citing papers (Table 1.2 and Table 1.3 discussed below). This is likely because both development (well-cited) and the evaluation/usage (well citing) of a mechanism requires knowledge from a range of different fields, making it an interactively collaborative process.

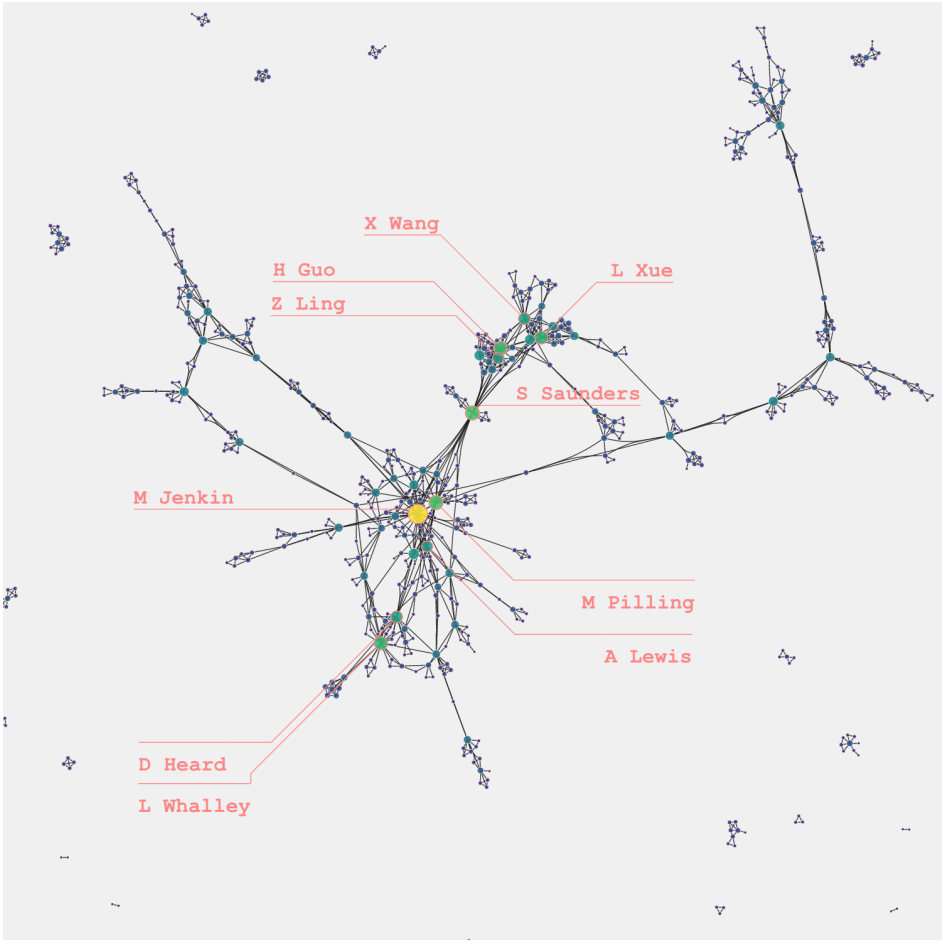

M Jenkin	39
S Saunders	25
M Pilling	25
H Guo	24
L Whalley	23
L Xue	22
D Heard	19
X Wang	19
Z Ling	18
A Lewis	17

Figure 1.5: **Degree Centrality.** In applying the degree centrality to the co-authorship network, it is possible to pick the authors with the greatest number of papers, of which the top 10 have been listed.

Directed Degree

For graphs where link direction holds an inherent meaning regarding their representation (for example in the citation graph an outward link symbolises that paper citing the one that the link points to), it is possible to further divide the degree centrality metric into inwards and outward links. This can allow us to separate items which provide a large number of lots of information (in-degree) and those who collate or collect it (out-degree). In applying these metrics to the directed citation graph, it is possible to get an insight into the core MCM development papers (Table 1.2) and separtate them from those which make use of the mechanism as part of a greater study (Table 1.3).

Protocol for the development of the Master Chemical Mechanism, MCM v3 Part A tropospheric degradation of nonaromatic volatile organic compounds	Saunders et al. [2003]
Protocol for the development of the Master Chemical Mechanism, MCM v3 Part B tropospheric degradation of aromatic volatile organic compounds	Jenkin et al. [2003]
Development of a detailed chemical mechanism MCMv3. 1 for the atmospheric oxidation of aromatic hydrocarbons	Bloss et al. [2005]

Table 1.2: **In-Degree of the citation network**: The top 3 most cited papers.

The MCM v3.3.1 degradation scheme for isoprene	Jenkin et al. [2015]
Atmospheric photochemical reactivity and ozone production at two sites in Hong Kong Application of a master chemical mechanismphotochemical box model	Ling et al. [2014]
HOx budgets during HOxComp A case study of HOx chemistry under NOxlimited conditions	Elshorbany et al. [2012]

Table 1.3: **Out-Degree of the citation network**: The top 3 most citing papers.

1.3.2 Closness Centrality

Often within a network, we are interested in how easy it is to to get information from one node to every other node. This is what the closeness centrality tells us. To calculate a nodes closeness we begin by taking the reciprocal sum of all the Dijkstra paths[5] to every other node [poliaktiv, 2011; Sabidussi,

[5]The shortest available path.

1966]. This gives is a representation of how far information from a certain will need to travel to reach every other node. Such a metric has applications in intelligence gathering, telecommunications and word importance within key-phrase extraction [Krebs, 2002; Borgatti, 2005; Boudin, 2013].

> ***Example analogy:*** *If we take the UK rail network as an example, York station will have a high closeness value as it is well connected and central in location. This means it is easy to reach every other location when compared to other stations.*

For the co-authorship network, Figure 1.6, nodes have been coloured by their closeness value. Here a heat-map-like effect may be observed, showing that information between the dense Leeds-York cluster is easier to disseminate across all parts of the graph than that of localised branches of authors less involved with the development team. The results of the closeness centrality suggest that should a problem (bug) or improvement (update) occur, Michael Pilling would be the best served to pass that information to all other groups using the MCM.

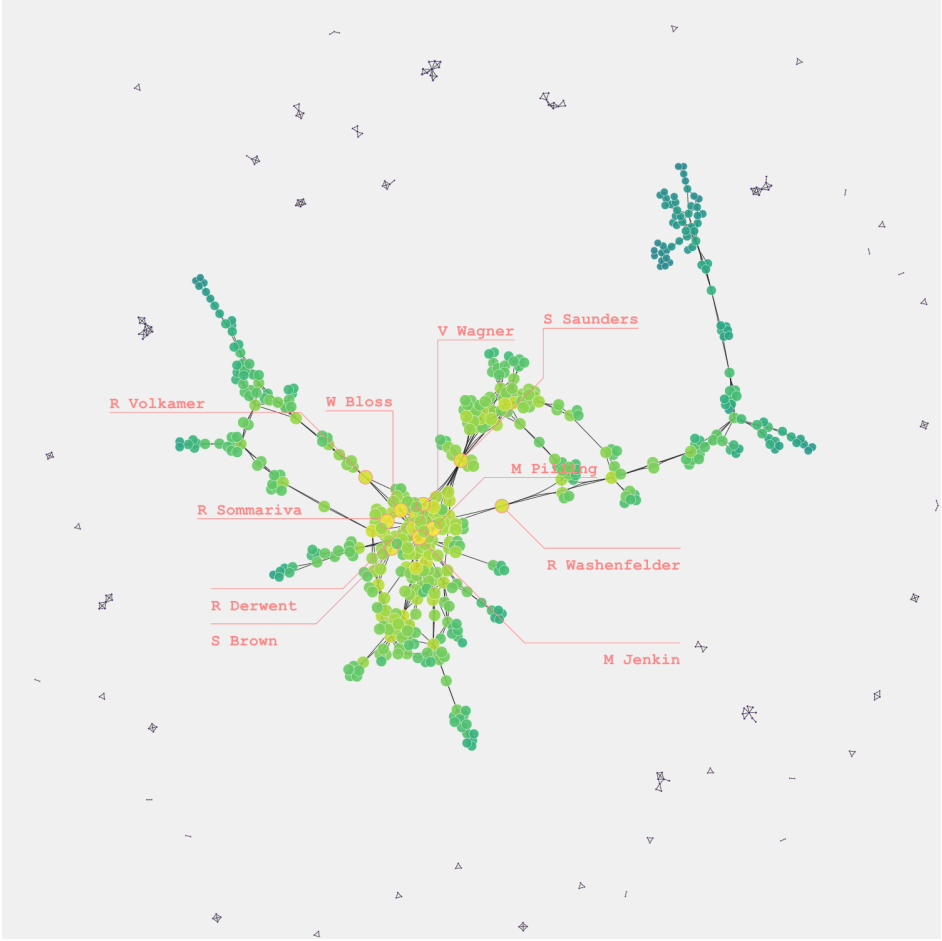

M Pilling	0.149995
M Jenkin	0.146532
R Sommariva	0.145251
W Bloss	0.144052
S Brown	0.142059
S Saunders	0.140176
V Wagner	0.139281
R Derwent	0.136450
R Volkamer	0.136184
R Washenfelder	0.135918

Figure 1.6: **Closeness centrality within the co-Author network.** Here a colour/size gradient is seen, with the nodes that are more central (in location) and better connected having a higher closeness than those in the peripheries - which are harder to get to.

1.3.3 Betweenness

In social networks, it is often important not only to know who has the greatest reach (closeness centrality) but also where bottlenecks or 'broker' positions occur. Nodes with a high betweenness control, or limit, the amount of information that can be transferred across the network. If a node lies on a geodesic (the shortest path between two other nodes), we may consider it a 'pivotal' node, due to its role within the network [Needham and Hodler, 2019]. Should such a node then be removed, the

overall flow of information incurs either a deviation, the information will either need to travel a longer (alternative) route or may not be able to reach its destination at all [Freeman et al., 1991; Freeman, 1977; Brandes, 2001; Borgatti, 2005]. Betweenness centrality is a count of the number of geodesics which pass through a node. If multiple 'shortest' paths are possible, this is accounted for within the denominator.

> ***Example analogy:*** *Expanding on the UK rail network analogy, Shrewsbury station serves the critical role of connecting many lines from England to Wales. In removing this station, routes from the Liverpool or Manchester to Cardiff will be greatly increased. Additionally, the Aberystwyth section of the line will then become isolated from the rest of the country.*

Authors with a high betweenness in Figure 1.7 are seen to lie along the joints between clusters. Here we can imagine that removing Li, Griffin or Liu can disrupt the overall flow of collaboration, potentially isolating the work of the Max Planck from that of everyone else. Similarly, Jenkin and Pilling can be seen as holding much of the Leeds cluster together. In removing them from the network (if for example, the refused to collaborate) it is possible to see how many of groups within the Leeds environment may not have worked together, with the cluster potentially separating into several smaller groups. Finally, we see Saunders (Australia), who served to introduce the MCM to the Chinese atmospheric community. In removing her from the network, it can be seen that much of the collaboration which exists would have been significantly less likely.

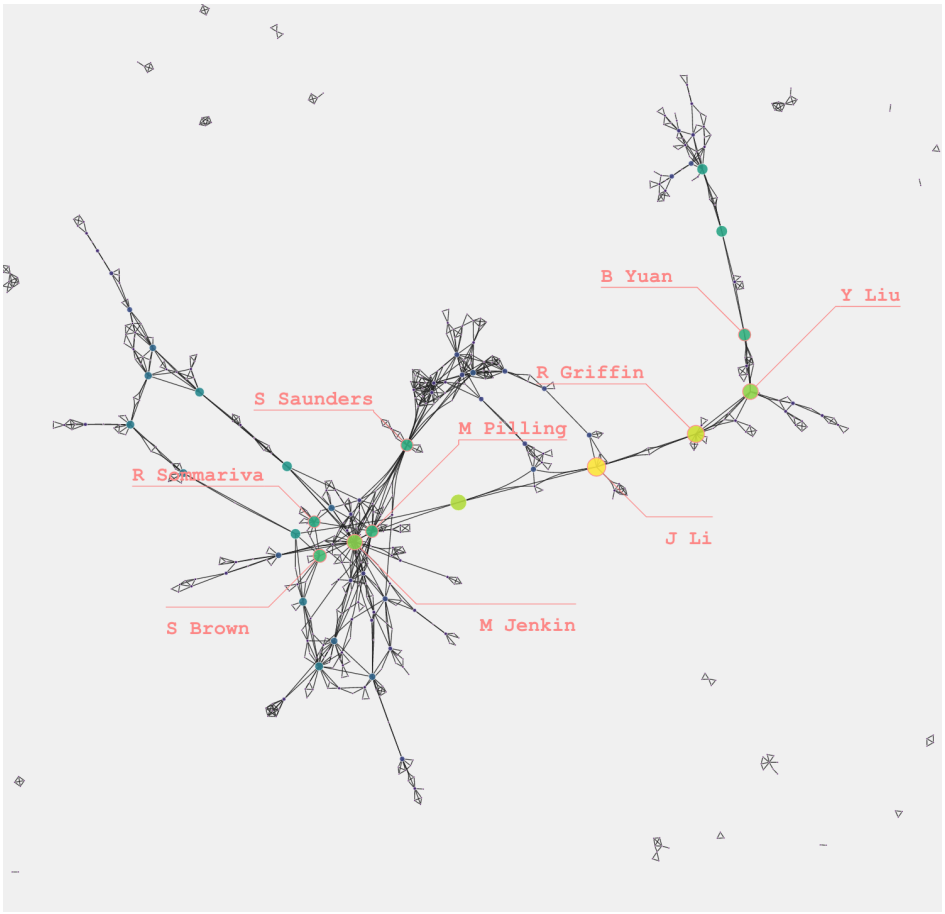

J Li	0.180998
R Griffin	0.162558
R Washenfelder	0.153024
Y Liu	0.142194
M Jenkin	0.139818
S Brown	0.110188
M Pilling	0.102816
B Yuan	0.099914
S Saunders	0.097255
R Sommariva	0.094757

Figure 1.7: **Betweenness centrality within the co-Author network.** Nodes which lie on a pivotal position (connecting/bottleneck) tend to have a high betweenness value due to their crutial role within the network.

1.3.4 Spectral methods and matrix analysis

Graphs can often be represented in the form of relationship (adjacency) matrixes (ref Chapter 1). This allows us to apply the theory of linear maps, such as eigenvectors and values, to stochiometric data in matrix form. Such methods have been around since the 1950s, [R. Seeley, 1949], but mainly became popular with the release of Larry Page's page-rank algorithm [Page et al., 1999] - the algorithm that began google. These methods, in addition to the HITS algorithm Table 1.3.4, make use of a graphs

native matrix representation to calculate node importance. Spectral algorithms can be broken down into four categories [Vigna, 2016]:

	No Normalisation	Row Normalisation
No Damping	Eigenvector [Bonacich, 1987, 2007]	Markov Chain Steady State [R. Seeley, 1949]
Damping	Katz [Goh et al., 2001]	Total Effect Centrality PageRank [Page et al., 1999]

Here damping terms represent the probability of moving to the new random starting position, allowing for the user to 'randomly select a new webpage' or leave an isolated cluster. The normalisation of the matrix does not affect the node ranking, but merely adjusts the numerical output of the algorithm. It is for this reason that its overall practicality may be debated [Vigna, 2016]. Since page rank is the most common of these methods and allows for a tune-able degree of randomness within network propagation. This is discussed in more detail in the next subsection.

Hypertext Induced Topic Search (HITS)

A common eigenvector algorithm used for classifying webpages is the HITS algorithm. This helps categorise the role of a node as either a Hub or an Authority, [Kleinberg, 1999; Langville and Meyer, 2005; Kumar and Upfal, 2000]. Similar to the in and out-degree metrics, this algorithm separates nodes with many outgoing links (an authority) from those with many ingoing ones (an information hub). Overall this provides similar results to the in/out degree, although since it looks more on how information propagates across the network as a whole, it often provides more accurate, and different, rankings to simple degree analysis.

1.3.5 Page Rank

Arguably the best-known centrality algorithm is PageRank. This is a spectral method for measuring the transitive influence of a node, by taking the effect of neighbours and by their neighbours into account [Needham and Hodler, 2019]. The page rank algorithm was initially developed to provide a better way of ranking web pages [Page et al., 1999]- here an important page is not only one of many links, but links to other important sources. In the context of academic papers, that same paper also found that in predicting future citations, the page rank algorithm fared better than using the current citation count of a paper. To explain how this works, we will look at the mathematics behind the algorithm, and then eventually apply it to the co-authorship graph in subsubsection 1.3.5.3

1.3.5.1 The Google Matrix

To solve for page rank, a google matrix must first be constructed. Once done this is iterated until convergence is reached.

To build a google matrix, we must first generate a dyadic link map of the graph[6] - its adjacency matrix $A_{i,j}$ (i, j are the source target indexes). This is then converted into a Markov matrix $M_{i.j}$ by dividing each column j by the sum of the total outgoing links of node j, Algorithm 1. Species with no outgoing links (sinks), are adjusted with either a personalised list of values or the constant $1/n$, (where n is the number of nodes) to replace the zero-sum columns. This produces a normalised[7] matrix of Markov chains representing the fractional production for node j from all other nodes.

Algorithm 1 Adjacency to Markov matrix.

1: Obtain graph adjacency matrix, $A_{i,j}$.
2: **repeat**
3: **for each** $j \in$ columns **do**
4: $M(:, j) \leftarrow A(:, j)/\Sigma_{i=1,n}A(j, i)$
5: **end for**
6: **until** $\Sigma_{i=1,n}M(i, j) = 1$

The google matrix $G_{i,j}$ can now be defined using Equation 1.1. Cyclic reactions and nodes that only point towards each other within a group can 'trap' the user, increasing their ranks. To account for this, a damping factor, typically $\beta = 0.85$, is used. This defines the probability that the user follows a link, and that for which they randomly select another page: $(1 - \beta)$ [8]. The damping factor used varies greatly with the application, with values such as $\beta = 0.694$ having been found optimal for the use of biological data [Hobson et al., 2018].

$$G_{i,j} = \beta M + \frac{1 - \beta}{n} \tag{1.1}$$

β - *Probability the user follows a link*
$(1 - \beta)$ - *Probability the user does not follow a link (teleportation)*
n - *Number of items / species*
M - *Normalised markov matrix*

[6] In sociology a dyad is a group of two people - the smallest possible social group.

[7] $\Sigma_{i=1,n}M(i, j) =$ unity

[8] Also known as teleportation.

1.3.5.2 Solving the algebra

Once defined, the google matrix is solved by propagating a one's vector, r of length n, where n is the number of species using Algorithm 2.

Algorithm 2 Solving the google matrix linear algebra

1: Define value vectors $\bar{r}_t$ and $\bar{r}_{t+1}$:
2: $\bar{r}_t = [1_1, 1_2, ..., 1_n]$, $\bar{r}_{t+1} = [0_1, 0_2, ..., 0_n]$
3:
4: **while** $||\bar{r}_{t+1} - \bar{r}_t|| > \epsilon$ **do**
5: $\bar{r}_{t+1} \leftarrow M.\bar{r}_t$
6: $\bar{r}_t = \bar{r}_{t+1}$
7: **end while**

This is repeated until a pre-defined tolerance, ϵ is reached. For best results, this can be set to just under the numerical precision of the programming language/hardware.

For smaller systems, it is possible to use the LAPACK [lap, 2019] library, as used by [Oliphant, 2006]. For a large network, however, the computation of an $n \times n$ matrix can be very memory inefficient for small machines. It is then possible to apply the methods as described above using a sparse matrix on per-node bases as can be seen within the scipy implementation of the networkx source code [Jones et al., 01 ; Hagberg et al., 2008].

1.3.5.3 Prediction

As the PageRank algorithm is a physical representation looking at how quantities 'flow' within a network, it can be used to identify not only the bottlenecks (betweenness centrality) but also any nodes which are connected well within the network. As the flows between a node are somewhat governed by the number of links it contains, the PageRank algorithms tend to correlate, but not a dependance, on the betweenness of a node. Figure 1.8 shows the PageRank algorithm to identify important authors within each 'cluster' or research group. Due to its propagating nature authors connected to these important nodes are often also of greater importance. An application of this can again be the determination of how to best spread new results or information with the least number of people. *Note: if we only had one person we would probably use the node with the highest closeness centrality.*

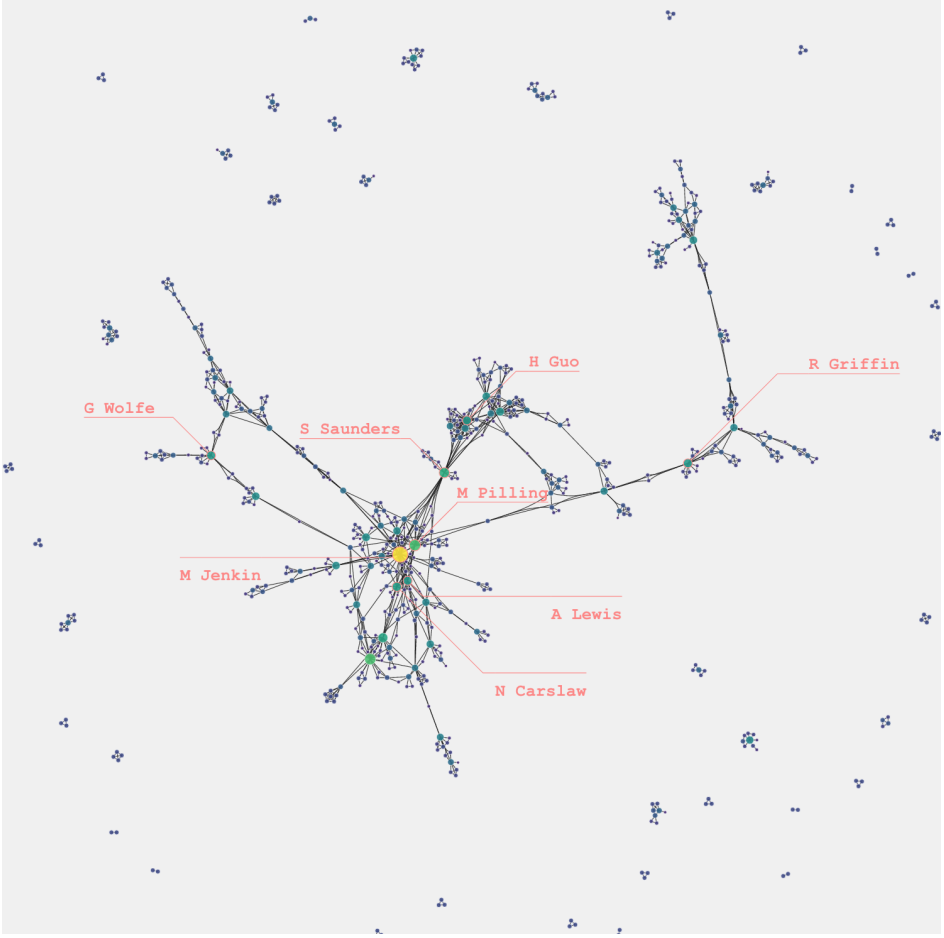

M Jenkin	0.010435
L Whalley	0.006589
M Pilling	0.006488
S Saunders	0.005591
D Heard	0.005192
N Carslaw	0.004833
H Guo	0.004594
G Wolfe	0.004523
A Lewis	0.004508
R Griffin	0.004500

Figure 1.8: **Page Rank centrality within the co-Author network**.

1.3.6 Conclusions

In this section, we have explored the use of centrality metrics to provide us with information on an unweighted co-authorship network of the MCM. Having used these to demonstrate the different roles that may be extracted from a node, we can move on to applying them to a chemical mechanism. In the next section, a global set of metrics will be used to determine the network type/structure of the MCM. Once this has been done, graph construction using simulation results (a weighted graph) will be looked into in subsection 1.5.1.

1.4 Classifying the Master Chemical Mechanism network

Having shown that graph metrics can help the roles of individual nodes within the network, I will now apply them to a chemical system. Since computational efficiency and resources are often a limiting factor, many applications of the MCM only require a small subset of the entire mechanism. For this reason, it may be of interest to compare these against each other, in an attempt to classify the type of network the MCM chemistry falls under. In this section, we apply graph theory to the entire MCM network, to determine its defining characteristics. This is achieved through the analysis of several hundred randomly selected subsets of the MCM.

1.4.1 Network density

Network density is the easiest to understand. Visually this can induce complexity and obscure aspects in a graph, mathematically it can greatly increase the computation time for metrics or algorithms. By definition, we can define network density as a measure of how well connected a node is to every other node, mathematically it is the ratio of edges against the total number of possible edges for a complete graph[9] of the same size. In chemical terms, we can use this to determine the sparsity of the graph (which has applications on model integrator selection) and give us insights on the chemical structure. In Figure 1.9 the addition of more species (nodes) results in an overall decrease in the node-edge ratio - it's density. This suggests a modular or hierarchical structure, where new species directly react only with a set number of species, and not the entire mechanism. An explanation for this is that the addition of larger species introduce new branches within the chemistry, which then need to be oxidised before they are small enough to react with the species from a different branch. Since these branches are somewhat isolated from the rest of the chemistry, they decrease the network density, even though their addition may increase the amount of chemistry that occurs within it.

[9] A complete graph is one where every node is connected to every other node.

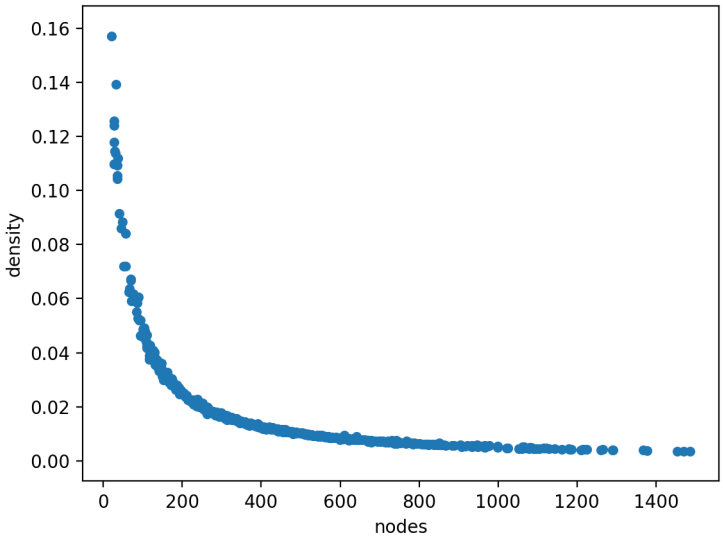

Figure 1.9: **How the MCM graph density scales with number of species.** A figure showing that an creasing the number of species within a mechanism subset results in an increased model sparsity (decreasing density).

1.4.2 Small world Phenomena

Within the biological or social sciences the small world phenomenon, colloquially known as 'six degrees of separation', is a common occurrence within network structure [Watts and Strogatz, 1998]. Such networks have a large number of localised clusters (cliques) all with a short path length between their elements [Humphries and Gurney, 2008]. This makes it easy to reach all parts of a network with only a couple of hops/reactions. In the initial interactive explorations of graph visualisation, it was found that in selecting the reactions of a node, and consequently the reactions of all the nodes which react with them, very quickly a large proportion of the network was highlighted. This suggests that the network may follow the small world phenomena, especially as it is a sparse network, subsection 1.4.1.

One of the possible methods for establishing the small world-ness of a graph falls under the of the omega (ω) coefficient:

$$\omega = L_r/L - C/C_l \tag{1.2}$$

Here C is the average clustering coefficient and L, the shortest path length of the graph. Comparing these with the average shortest path length, L_R, and clustering coefficient C_l (as calculated using an equivalent random and lattice graph) gives the above equation. The output is a result between positive and negative one {-1,1}, where a value of 0 suggests the graph exhibits perfect small world-ness.

In assessing the network structure of the MCM, a Monte Carlo (random) approach was taken to

extract several hundred subsets from the entire mechanism. For each of these, the omega coefficient was calculated and plotted in Figure 1.10. Here it is seen that subsets with a small number of species (for example those derived only from Methane or Ethane) exhibit a more lattice-style graph, with the majority of the networks showing a more random network structure. All the results, however, show a prevalence of small-world features over any of the alternative network structures - they are closer to 0 than 1 or -1. This reflects the idea that large species react locally, forming branches (REF VIS CHAPTER), before oxidising to smaller species with more reactions. This result is also seen within the Reaxys chemical database [Jacob and Lapkin, 2018].

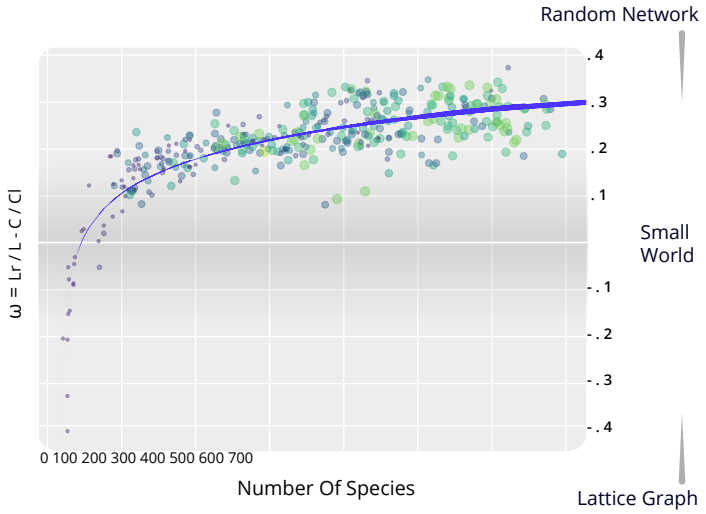

Figure 1.10: **A figure showing the small worldness for many Monte-Carlo selected MCM subsets**. The network structure of these is then assessed using the omega coefficient, with [-1,0,1] corresponding to the perfect lattice, small-world and random network structure. Here Node size and colour represents the number of reactions in the subset and the number of primary VOCs (blue=small, green=large).

1.4.3 Power Law and Scale-free graphs

In real-world applications, it is common to have a hierarchical structure. These are often seen in the increase of citation counts in academic papers [de Solla Price, 1965], email threads [Ebel et al., 2002] and the world wide web [Needham and Hodler, 2019]. Unlike random or small-world graphs, scale-free graphs take a hub-and-spoke structure (Figure 1.11), which follows a power-law distribution - that is that scaling probability $p(x) \propto x^{-\alpha}$, where α is a constant and known as the scaling parameter.

Broido and Clauset [2019] suggests that scale-free networks are rare, and often misdiagnosed with incorrect tests, or the misinterpretation of power-law features in a network. Similarly, Clauset et al. [2009] suggests that even if the data distribution of a graph is well represented by the power-law distribution, in many cases a logarithmic or exponential distribution may have a better fit.

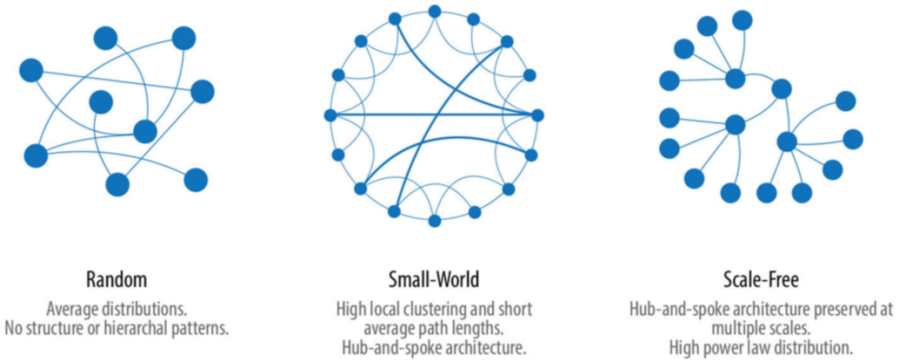

Figure 1.11: **The different network structures**. A visual depiction of the different graph structures. Source: Needham and Hodler [2019]

To assess the best distribution for describing the monte carlo subsets of the MCM I use the Kolomogorov-Smirnov statistic [Press et al., 1992]. This calculates the maximum distance D between the selected cumelative distribution function $S(x)$ (In our case the Logarithmic, Exponential and Power Law) of the data and the fitted model $P(x)$:

$$D = \max_{x \geq x_{min}} |S(x) - P(x)| \tag{1.3}$$

Using the MCM subsets from before Figure 1.12 shows that out of the three tested distributions, the MCM is best represented as a power-law distribution. Although this is not entirely within the chosen 5% significance, it is highly indicative that some aspects of the network are scale-free.

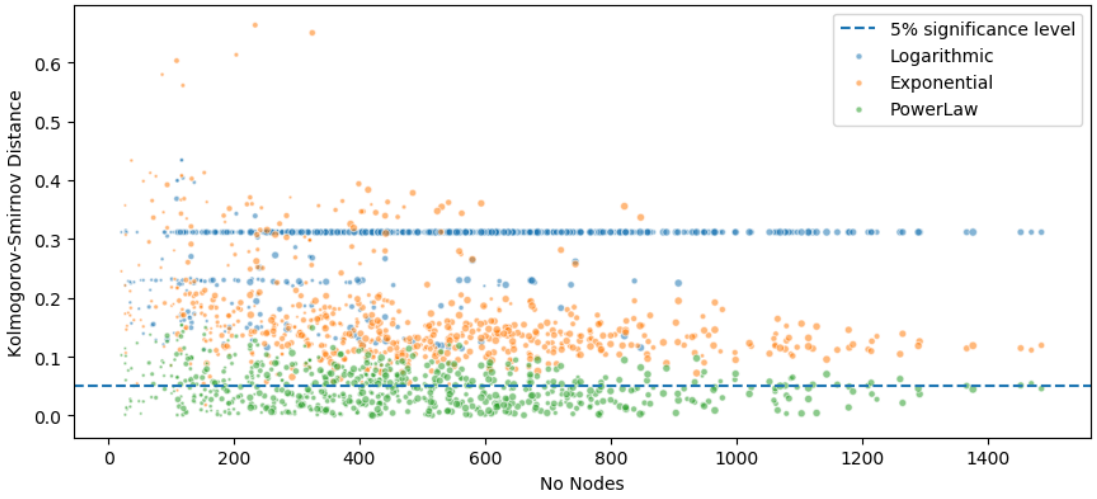

Figure 1.12: **Comparing the MCM subsets against a power law, logarithmic and exponential distribution.** The fit for different cumulative probability distributions of nodes in the MCM network is compared to determine the type of network hierarchy the chemistry follow. This is done by comparing the distance of the calculated distribution of data against a perfect one using the Kolomogorov-Smirnov test. The closer the two distributions are the better the fit.

1.4.4 Describing the MCM network

To conclude the MCM network exhibits both small world and scale-free (power-law) characteristics. This agrees with previous knowledge about the apparent network structure (branch and core - ref CH1/2). Here large primary emitted hydrocarbons produce branches of a hierarchical nature, as they are progressively broken down into smaller species. Since smaller species are then able to react with a much greater range of species, they then begin to form a tightly connected core, which exhibits many small-world features. This can be seen as the densely connected region within the graphs in CHAPTER !.

Having classified the MCM network type, the next section will look at how MCM based simulation results can be converted into the graph structure for more in-depth analysis, section 1.6.

1.5 Graph Construction methodology

Thus far we have only applied a qualitative analysis on the relationships between species in a mechanism. Although this can educate us about the chemistry within a specific system, often a quantitative value for the rate of reaction between different species is required when undergoing scientific evaluation or policy advice. To obtain such results a chemical mechanism is placed within an atmospheric model, initial concentrations are supplied and the chemistry is propagated forwards[10] in time. Currently, there exist three main model diagnostics which we may use to analyse the importance or role of a species from a simulation (model) output.

1.5.0.1 Concentration time series

The simplest of these methods look at the abundance of a species at a specific point in the atmosphere - its concentration. As time moves forwards, chemicals within the atmosphere undergo a range of reactions which result in the making and breaking of bonds - thus the changing from one species to another.

Using the species concentration as a metric, we can map how it changes over time, and how in changing the initial concentrations of a simulation can produce different results. This can be useful for looking at a range of possible scenarios and evaluating the potential outcome after a pre-determined amount of time. An example would be through the use of policy-based simulations to predict changes in ...

Using a simple example from a Methane only subset of the MCM (Figure 1.13), it is possible to observe the inverse relationship between NO_2 and NO using only their concentration profiles. Here nitrogen

[10] Or backwards if the adjoint is used. (see section PAGERANK APPLICATIONS)

monoxide reacts with a RO_2 species to produce an RO and nitrogen dioxide. This then photolyses back to nitrogen oxide, releasing oxygen which may go on to form ozone (REF NOX CYCLE IN INTRO). The latter part of this reaction is dependant on photons and therefore can only occur during daytime (mostly).

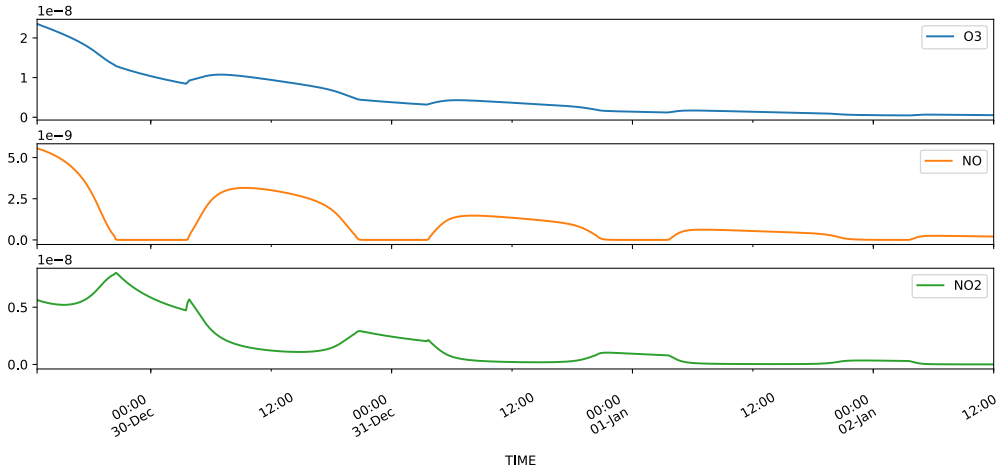

$$\mathrm{NO} \underset{h\nu}{\overset{\mathrm{RO_2}}{\rightleftharpoons}} \mathrm{NO_2}.$$

Figure 1.13: **A concentration time series from a simple methane-only simulation.** This is the simplest method for identifying changes in species within a model simulation. This multi-plot shows the changes in concentration profiles for all initialised species (NOx:10ppb; CH_4:20ppb; O_3:30ppb) following an initial 3 day spin-up to steady state.

1.5.0.2 Rate of Production and Loss

Analysing the concentration-time profiles allows the comparison of how a series of scenarios or runs change concerning their initial conditions and simulation length. Although these can tell us how, and how much, each species changes over time it does not rank or quantifies the specific reactions to which this may be attributed. Rate of Production Analysis (ROPA)[11] provides a method for establishing the total contribution from each reaction by calculating the change of concentration (concerning time) for the produced species - the instantaneous reaction Flux.

$$r_1 = \eta A + \omega B \xrightarrow{\kappa_1} C \qquad \text{Reaction 1} \tag{1.4}$$

$$f(C) = \frac{\delta C}{\delta t} = [A][B]\ \eta\omega \times \kappa_1 \qquad \text{Instantanious Flux } (\Gamma) \tag{1.5}$$

Here A, B and C are example species; [A],[B] and [C] are species concentrations; η and ω are rate coefficients and κ is the rate of the reaction.

[11] and loss

Using a sample simulation representative of the conditions within Beijing (an urban environment), we explore the reactions contributing to the production and loss of CH_3CO_3, Figure 1.14 at noon. The main reason for this specific example is that it can demonstrate how isolating a specific cause for the change within a species concentration may prove difficult in the context of atmospheric chemistry. Here we have many similarly weighted production and loss reaction, including that of peroxyacetyl nitrate (PAN) and nitrogen dioxide: $CH_3CO_3 + NO_2 \rightleftarrows CH_3C(O)ONO_2$ (PAN). The reversible nature, coupled with its near-identical production and loss fluxes produce a very small net change within our species of interest (CH_3CO_3). Although this may be seen by calculating the cumulative flux between individual species, it is evident that simply looking at the concentrations or highest-ranking reaction fluxes may not be the best method of determining influence. To account for this we can look at how a change in one species can affect another using the Jacobian method.

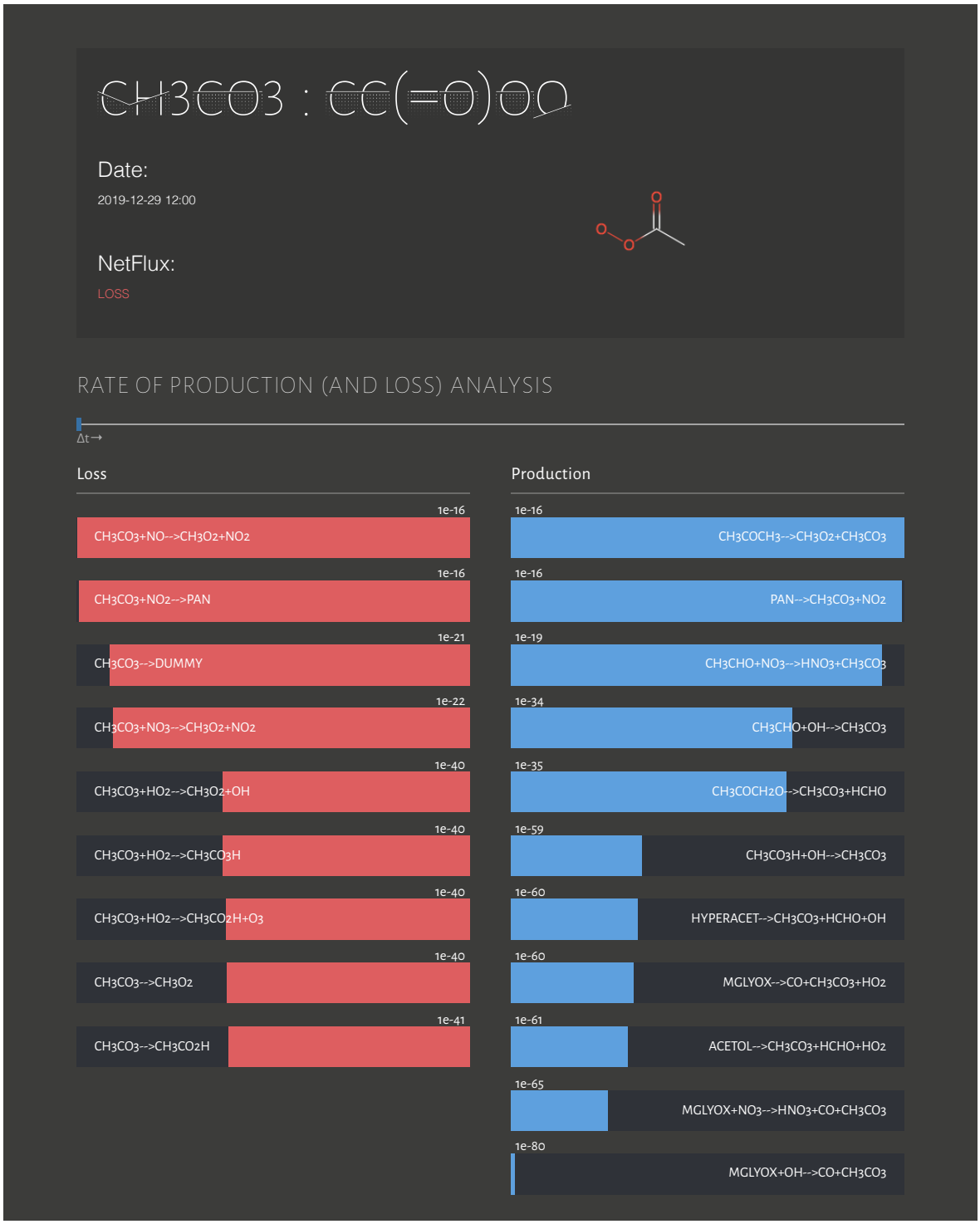

Figure 1.14: **Rate of production and loss analysis plot for CH_3CO_3 exhibiting a net loss (daytime).** An example ROPA plot from a simulation representing the chemistry within Beijing. This is used to identify the usefulness and weaknesses of using such a method.

1.5.0.3 The Jacobian

"The Jacobian [matrix] generalises the notion of gradient to describe the sensitivity to a vector" - Brasseur and Jacob [2017]. That this means is that in taking the partial derivatives of each reaction flux (e.g. from Equation 1.5), we can construct a representation of the influence each species has on itself - for example, the influence of species A on C and B on C (Equation 1.6-1.7).

$$\frac{\partial}{\partial A} \cdot \frac{\partial C_{r_1}}{\partial t} = \eta\omega B\kappa_1 \qquad \Gamma \text{ influence from A} \tag{1.6}$$

$$\frac{\partial}{\partial B} \cdot \frac{\partial C_{r_1}}{\partial t} = \eta\omega A\kappa_1 \qquad \Gamma \text{ influence from B} \tag{1.7}$$

These partial equations can then be aggregated for all reactions that contain the two species - taking the effect of species B on species C, for example, produces Equation 1.8. Using these aggregate sums it is now possible to construct a pairwise relational matrix describing the influence each species has on every other species- Equation 1.9. This is known as the jacobian matrix and is what is used to propagate the chemistry within a simulation forwards in time.

$$\mathbf{J}_{C,B} = \frac{\partial f(C)}{\partial B} = \frac{\partial}{\partial B} \cdot \left(\frac{\partial \Sigma_{r_1}}{\partial t} + \frac{\partial \Sigma_{r_2}}{\partial t} + \cdots + \frac{\partial \Sigma_{r_n}}{\partial t} \right) \tag{1.8}$$

$$\mathbf{J}_{i,j} = \begin{bmatrix} \frac{\partial f_1}{\partial v_1} & \frac{\partial f_1}{\partial v_2} & \cdots & \frac{\partial f_1}{\partial v_n} \\ \frac{\partial f_2}{\partial v_1} & \frac{\partial f_2}{\partial v_2} & \cdots & \frac{\partial f_2}{\partial v_n} \\ \vdots & \vdots & \ddots & \vdots \\ \frac{\partial f_n}{\partial v_1} & \frac{\partial f_n}{\partial v_2} & \cdots & \frac{\partial f_n}{\partial v_n} \end{bmatrix}^{n,n}_{i,j=1} \tag{1.9}$$

1.5.1 Graph construction methodology for simulated data

Having covered the general definition of a Jacobian matrix and how it is constructed, we can now apply it to the context of mechanism analysis and comprehension. The first analogy that needs to be made is that for the flux, we have a the first differential of a specific reaction in time. If we consider the change in a species concentration as a 'displacement', we can think of the flux as its 'velocity'. Similarly, the Jacobian provides us with a description of how the individual flux of a species changes concerning the concentration (or displacement) or another species (the second-order partial differential). This is analogous to the acceleration of the object or particle we first displaced. In using the jacobian, we have constructed a relational matrix which outlines the effect a 1% change of a species has on all other species - a concept which is the foundation of the connectivity method (a mechanism reduction technique where all but essential and important species are removed), [Turányi and Tomlin, 2014].

Since the format of a jacobian is already in the form of a relational matrix, it can easily be converted to a weighted adjacency matrix, and then directly into the graph format. Since it only considers the aggregated influence between species, much of the work that would otherwise be needed to convert a mechanism into a graph format has already been done. To make use of the Jacobian matrix, several extraction algorithms were written for an updated version of the Dynamically Simple Model of Atmospheric Chemical Complexity (DSMACC) [DANDSMACC,DSMACC ref], as discussed in INTRODUCTION. Here we edit the kinetic pre-processor output, [**?**] to release the values of the Jacobian Matrix and return them at each model timestep for analysis. The process for how this is done is described in subsection 1.5.2.

A note on using the Flux instead of the Jacobian

Depending on the model setup or the users' capabilities, extraction of the jacobian matrix for each timestep may not be possible. In many cases, the reaction rates and concentration may still be available, allowing for the calculation of reaction fluxes throughout the simulation. If this is the case the total flux can be calculated using the method described in Equation 1.5. From this, an edge-weighted by a reaction flux can be created from every reactant to each product. This generates a multi-graph[12] which may be simplified by taking the net flux value for all edges between two nodes.

However, the potential for human/coding error, additional simplification and a non-explicit definition of the contribution of each species make the use of a Jacobian much more efficient in network generation from a chemical mechanism.

[12] A graph with multiple edges between nodes

1.5.2 A practical Example using the MCM

Taking a single equation from the MCM we may calculate the jacobian relationships between species and convert them into a graph. A randomly chosen ethane reaction (Equation 1.10) from a simple mechanism was chosen. It must be noted that in general it is unusual in the MCM that alkyl radicals react rapidly and extremely well with O_2 to from stabilised peroxy radicals, [Jenkin et al., 1997]. In general, the reaction would consist of the following two steps: $C_2H_6 + OH \xrightarrow{\kappa_1} C_2H_5\cdot + H_2O$ and $C_2H_5\cdot + O_2 \longrightarrow [\kappa_2]\, CH_2H_5O_2$.

$$C_2H_6 + OH \xrightarrow{\kappa_3} C_2H_5O_2 \tag{1.10}$$

For simplicity in this example, this will be the only equation for our mechanism. The resultant Flux Equation 1.11 and resultant Jacobian Equation 1.12 may be calculated.

$$\Gamma = [C_2H_6][OH]\kappa_1 \tag{1.11}$$

$$\mathbf{J}_{i,j} = \begin{bmatrix} \frac{\partial f_{[C_2H_6]}}{\partial t\ \partial[C_2H_6]} & \frac{\partial f_{[C_2H_6]}}{\partial[OH]} & \frac{\partial f_{[C_2H_6]}}{t\partial[C_2H_5O_2]} \\ \frac{\partial f_{[OH]}}{\partial t\ \partial[C_2H_6]} & \frac{\partial f_{[OH]}}{\partial t\ \partial[OH]} & \frac{\partial f_{[OH]}}{\partial t\ \partial[C_2H_5O_2]} \\ \frac{\partial f_{[C_2H_5O_2]}}{\partial t\ \partial[C_2H_6]} & \frac{\partial f_{[C_2H_5O_2]}}{\partial t\ \partial[OH]} & \frac{\partial f_{[C_2H_5O_2]}}{\partial t\ \partial[C_2H_5O_2]} \end{bmatrix}^{3,3}_{i,j=1} \tag{1.12}$$

Since not all species react with all other species, we can remove reactions that do not exist. This forms a 'sparse' jacobian. Substituting numbers from a subset mechanisms containing the methane and ethane precursors, we get Equation 1.13.

$$\mathbf{J}_{i,j} = \begin{bmatrix} \frac{\partial f_{[C_2H_6]}}{\partial t\ \partial [C_2H_6]} & -2 \times 10^{-7} & 2 \times 10^{-7} \\ -0.1 & \frac{\partial f_{[OH]}}{\partial t\ \partial [OH]} & 0.1 \\ & & \frac{\partial f_{[C_2H_5O_2]}}{\partial t\ \partial [C_2H_5O_2]} \end{bmatrix}_{i,j=1}^{3,3} \tag{1.13}$$

This allows us to see two things. Firstly that with the absence of external intervention (e.g. emissions) the overall change of concentration is a conserved property. Secondly ...

Representing these relationships as a simple 'ball and link' style graph gives us Figure 1.15.

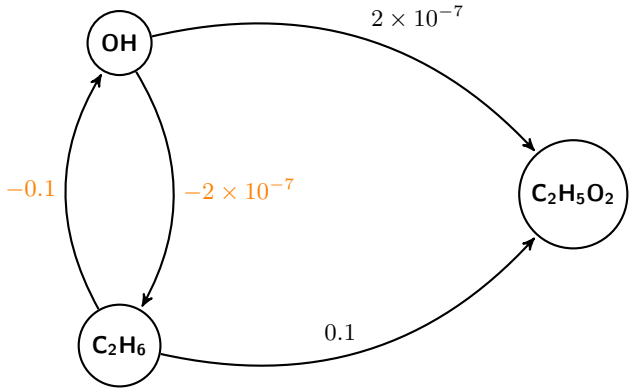

Figure 1.15: A graphical representation of Equation 1.13 derrived from the Equation 1.10

Converting the Jacobian into an adjacency matrix

Adjacency matrixes are a set of matrix representations which can be used in the construction of a graph. The relational data of the Jacobian matrix Equation 1.13 inherently holds such property and can be directly translated to produce a graph, Figure 1.15. However, we notice that some edge weights are negative, which although providing information about the chemical system provides no physical meaning in the graph structure.

It is for this reason that we can reverse the direction for all negative links to produce Figure 1.16.

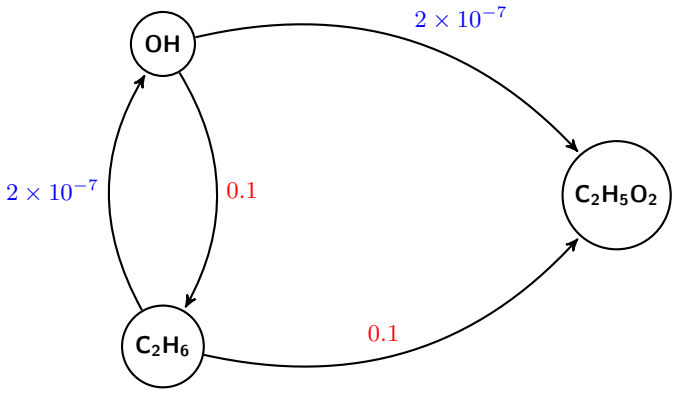

Figure 1.16: Reversing the directions on negatively weighted edges from Figure 1.15

For most graph algorithms this should be sufficient and is generally all that is needed. In some cases, it may, however, be noted that the graph may further be simplified to produce Figure 1.17. Although this is more practical, eigenvector metrics such as PageRank will automatically transfer the 'flow' of information down the system producing much the same overall result.

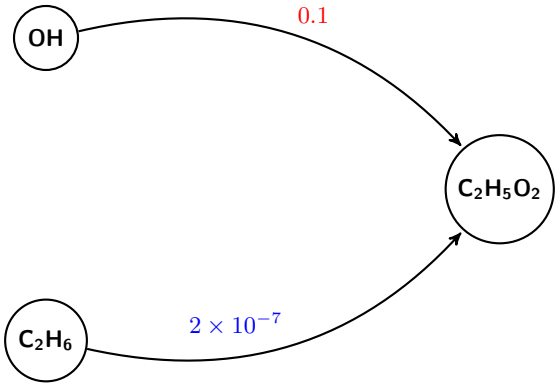

Figure 1.17: Simplifying Figure 1.16

1.6 Case study Example

In this section, the centrality metrics discussed in section 1.3 are applied to a range of scenarios. These range from polluted urban environments such as London [REF] and Beijing [REF], to marine and terrestrial forest- Cape Verde REF and Borneo REF. We determine the main drivers for the chemistry and compare the species which are important across each simulation.

1.6.1 Establishing Initial Conditions from observational data

Within experimental data assimilation, it is not uncommon to face problems which result in unreliable or missing data. These can range from anything as little as measuring below the instrument sensitivity

to powercuts and equipment damage/theft from the local wildlife. This can result in problems when analysing the results and combining them to create a simulation of the chemistry for that environment.

To overcome this, traditionally a combination of data filtration, smoothing and interpolation are required. Although it is possible to fit a diurnal profile, through iterative methods of comparison, and cubic splines, a much simpler way would be to use a Multi-Layer Perceptron Regressor model (MLPRegressor) as provided by sklearn, [**?**]. This is described below.

1.6.1.1 The origin of Artificial Neural Networks

The concept of a neural network originated within the field of neuroscience. In biological neurons, signals are sent through the use of electrical impulses using their synapses. When a sufficient number of signals are received within a short timeframe, a neurone will respond, often firing a range of its signals. Using this as a foundation,McCulloch and Pitts [1943] presented a computational model of the biological neuron - the artificial neuron. This has a series of binary inputs and produces a single binary output. This idea was later improved with the invention of the perceptron - a linear classifier which classifies categories by separating them with a straight line. Invented by Rosenblatt [1958], this was popularised as a device representative of a modern-day shallow neural network - [John Hay, 1960], Figure 1.18. Unlike the artificial neuron, however, the perceptron can take non-binary (numerical) inputs of an associated weight which allows for the computation of simple linear binary classification. Much like Logistic regression, the perceptron produces a positive or negative classification based on a certain threshold[13].

[13]It is worth noting that while a Logistic Regression classifier can output a class probability, the use of a hard threshold means that this is not done within the perceptron algorithm [Géron, 2017]

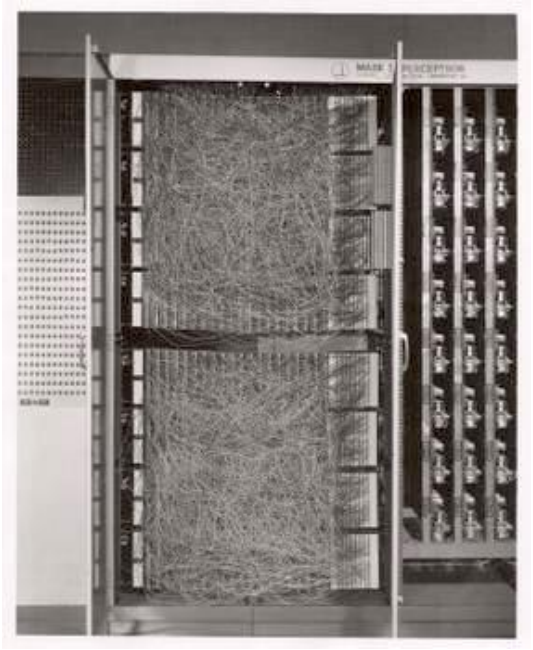

Figure 1.18: **The Mark 1 perceptron** Both software and hardware are different manifestations of a flow chart. The perceptron hardware accomplished what is now done using software. Source: Cornell [2020]

1.6.1.2 The Multi-Layer Perceptron

Limitations of the perceptron include the classification of complex patterns such as the XOR problem (where a category appears between two other categories e.g. 1|0|1 - this cannot be classified by a single linear split). In taking inspiration from nature, Figure 1.19, it is possible to overcome this with the use of multiple layers. This creates a deep ($>$ 2 two hidden (non-input) layers of perceptrons[14]) artificial neural network (ANN)

The multi-layer perceptron (MLP) model now represents a simple feed-forward network, much like a decision tree. However, unlike a decision tree, the MLP ANN can describe the probability a branch is taken using non-linear activation (threshold) functions. These are discussed in detail as part of **??**. The weighting thresholds for each neuron are then calculated by backwards propagation of results through the network until a suitably good result is produced.

> ***Example analogy:*** *Backpropagation can be likened to the iterative calibration of scientific instrumentation. In the field of atmospheric chemistry, laser-induced fluorescence is used to calculate species concentrations and reaction rates within the troposphere, [Dillon et al., 2006; Bloss et al., 2004]. Here the frequency of a laser can be adjusted in contrast with a known target (e.g. an amount of SO_2) to produce a response curve showing where the maximum resonance occurs.*

[14] These are sometimes referred to as Linear Threshold Units.

Similarly, a neural network can be 'trained' (calibrated). This is done through the use of a 'training dataset' - a set of input-output pairings which represent a random selection of 2/3rds of the total dataset. Next, the neurons within each layer (similar to the potentiometer dials on an instrument) are adjusted in sequence through the layers to match the known result (a standard of known concentration) to the input values provided. This process is repeated until for many iterations, or until a sufficiently 'good' prediction is attained for the entire training dataset (early termination). The power of ANNs comes from the ability to adjust neuron thresholds whilst moving both forwards and backwards through the network (Note: predictions of an MLP are still only passed forwards). Finally, model performance is evaluated against the remaining 1/3rd of the total dataset.

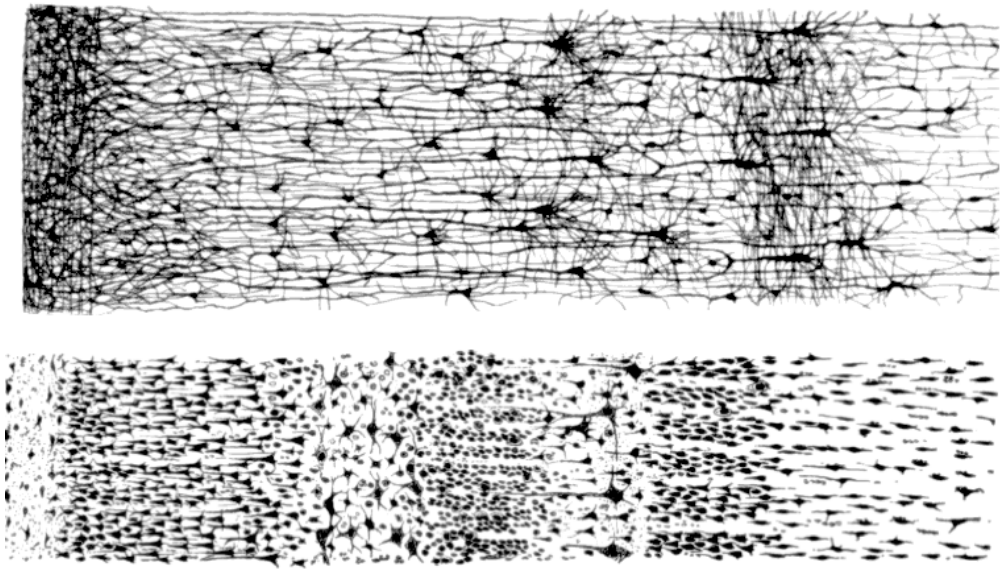

Figure 1.19: **The Human Cortex - A biological neural network.**. A vertical cross section of the human cortex between an adult (top) and 1.5 month old infant (bottom) showing a layer like structure with a change in depth (left to right). Source: Cajal [2020]

1.6.1.3 Applying the MLPRegressor to Observational data

In the application of any type of machine aided algorithms, it is important to evaluate the results provided. In this section, the results of 12 years of data collected as part of the [CAPE VERDE CAMPAIGN] are shown (these contain measurements spanning the entirety of 12 years, which produce the clearest tests for the algorithm). A MLPRegressor of 10 hidden layers, and a hyperbolic tan (tanh) activation function is used **??**. Additionally, the limited-memory Broyden–Fletcher–Goldfarb–Shanno (l-BFGS) solver (a quasi-newton method which minimises the inverse of the Hessian matrix[15] to steer

[15]The hessian is square matrix of second-order partial derivatives of a scalar-valued function/field describing the local curvature of a function (of many variables).

through space and obtain a solution) and an adaptive learning rate[16] is used.

The input of the regressor is in the form of a month and an hour, to represent each measurement. This allows it to find not only daily trends but also seasonal trends within the data. Once trained the regressor is then used to predict a diurnal profile for each month based on the observational data provided. For simplicity $\log_{10}$ values of the concentrations obtained have been used. To validate the results, the predicted MLPRegressor line is compared to a transparent scatterplot for all the results. In addition to this, a boxplot showing the IQR, median and mean (green line) plotted alongside to evaluate the predictor output.

In providing the MLPRegressor with both month and hour inputs, the data is not only fitted hourly (a diurnal average) but also across the seasonal/monthly cycles. This accounts for the variation between years and datasets. Since $\log_{10}$ values of the concentrations are used, species such as ozone (Figure 1.20) which for the Cape Verde dataset (clean air) do not change more than one order of magnitude, the effects of neighbouring months, which shift the diurnal away from the mean (the green line on the boxplot), can be seen. However since this is overall a small change, and the diurnals lie within the interquartile range, they still provide an adequate approximation. NO (Figure 1.21) on the other hand has a concentration change of several orders of magnitude. Here a distinct daytime peak is seen and is centred around a seasonally consistent mean value of the data. Here the multi-magnitude change in concentration also provides an effective silhouette of the data to which we may compare the fitted line. Finally the plots of NO_2 and iso-Pentane (Figure 1.22-1.23) vary both in diurnal magnitude and seasonally. Within these plots, changes in the data in the January and December months produce deceptively misleading results. Here although the diurnals are not symmetric, they fit well within the median, mean and interquartile range values, as well as the general data silhouette behind them. This suggests that it is a property of the data that we are fitting, and not that the regressor is producing incorrect results. It is however noted that for a more accurate seasonal prediction, periodic boundary conditions should be employed in the training dataset, where an additional two months are added before January and after December. As only a single value estimate from the summer region will be taken, this does not affect the result accuracy.

[16]Each time the model improvement fails to decrease the learning loss, the learning rate is reduced by 1/5. This means smaller jumps are made towards the curve peak.

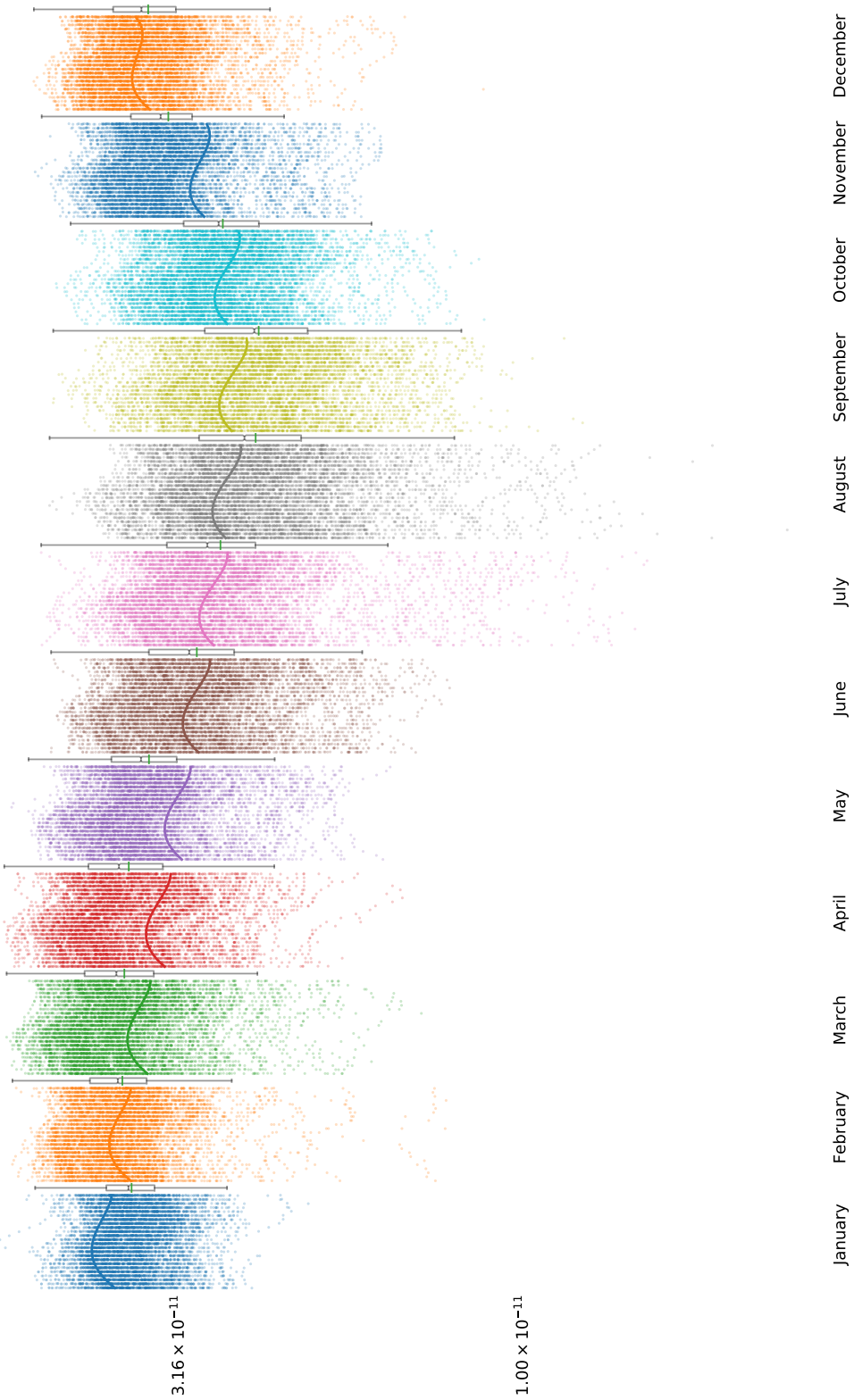

Figure 1.20: **Cape Verde MLP predicted and observational data of Ozone.** Each segment represents data from a different month. Within each month segment exists 24 hour segments to create a diurnal. Observational concentrations are plotted in the form of a translucent scatterplot and summarised using the boxplot on the right of the month segment. MLP predicted results are shown using the solid lines. Concentration in mixing ratio.

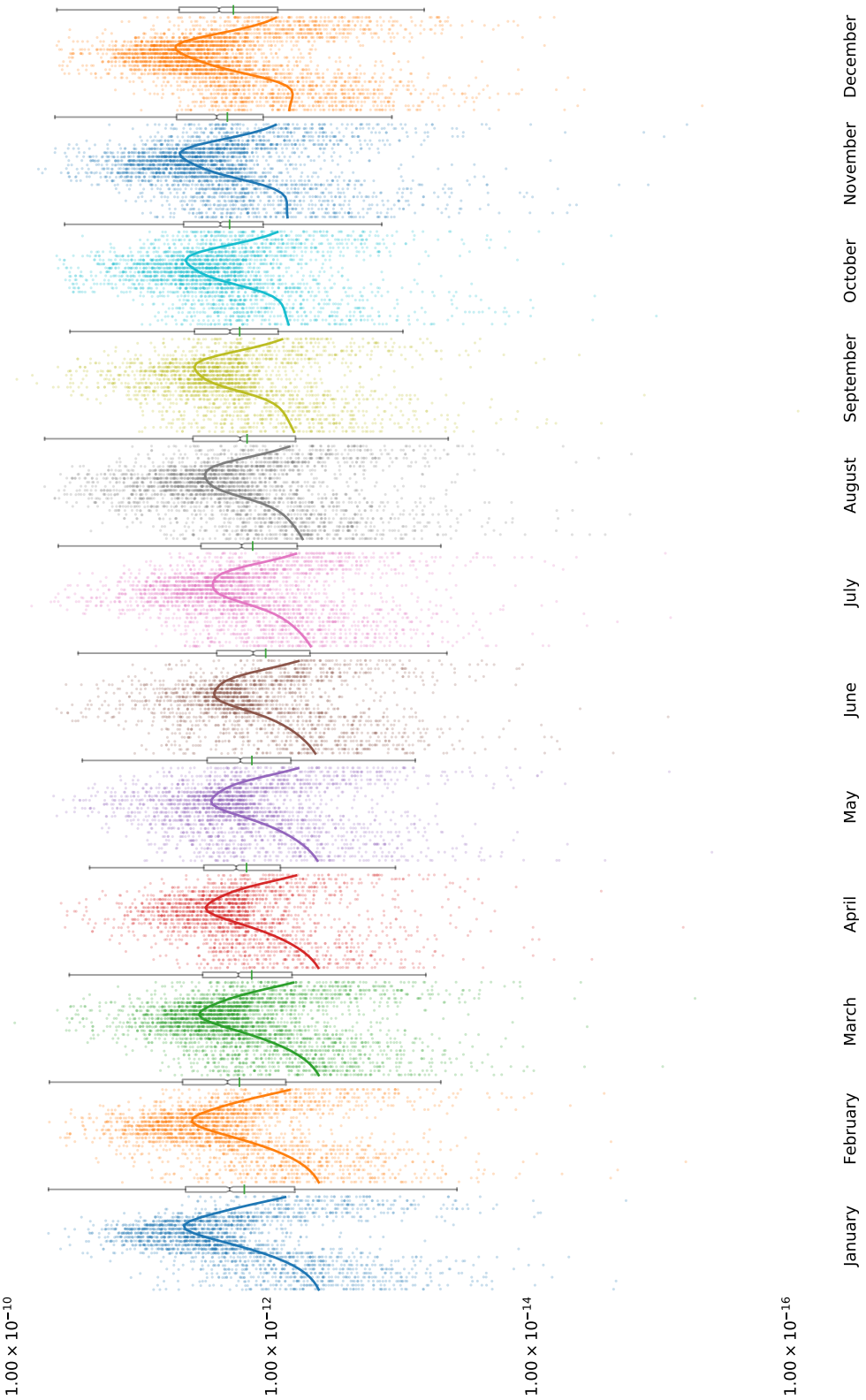

Figure 1.21: **Cape Verde MLP predicted and observational data of NO.** Each segment represents data from a different month. Within each month segment exists 24 hour segments to create a diurnal. Observational concentrations are plotted in the form of a translucent scatterplot and summarised using the boxplot on the right of the month segment. MLP predicted results are shown using the solid lines. Concentration in mixing ratio.

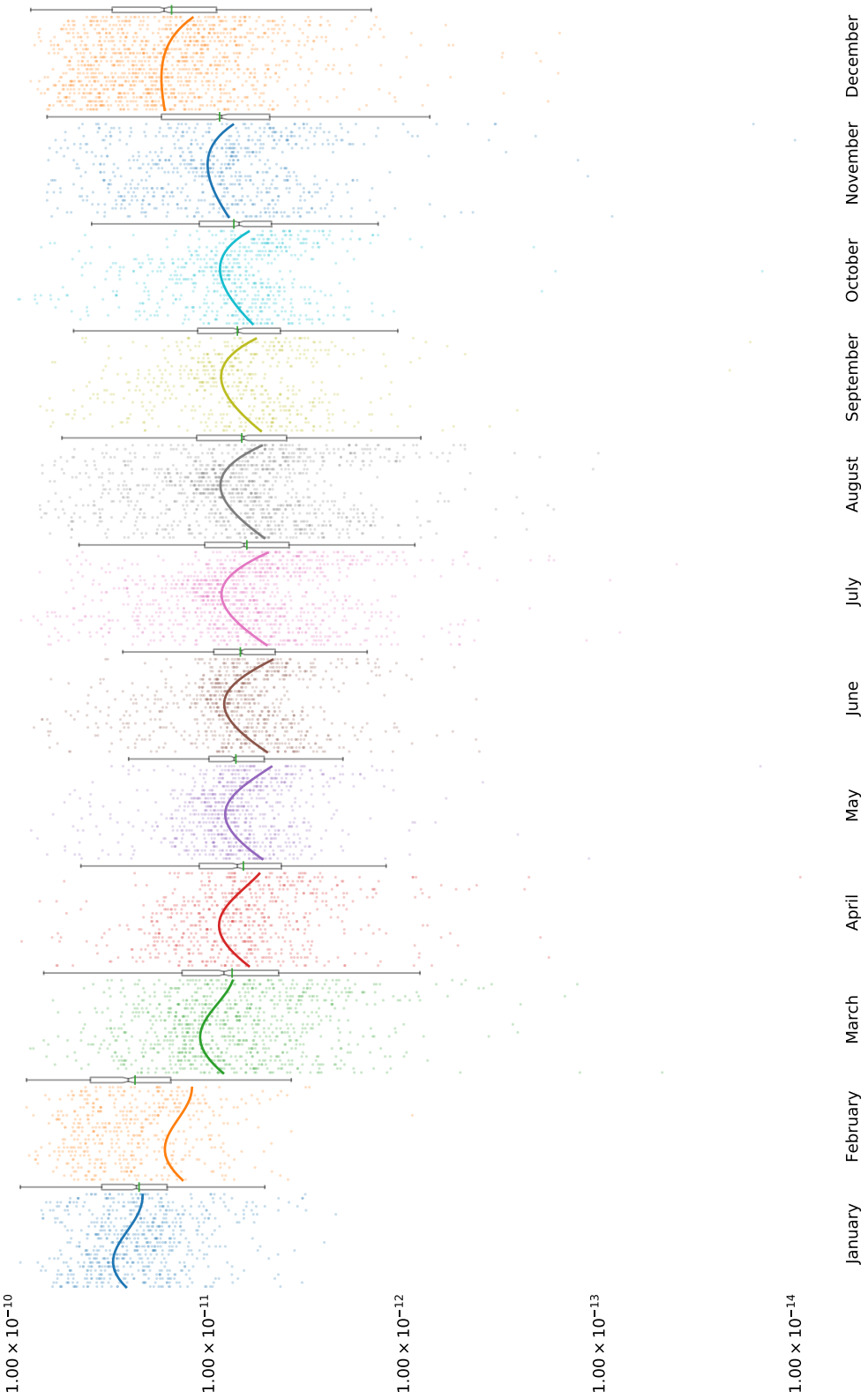

Figure 1.22: **Cape Verde MLP predicted and observational data of NO_2.** Each segment represents data from a different month. Within each month segment exists 24 hour segments to create a diurnal. Observational concentrations are plotted in the form of a translucent scatterplot and summarised using the boxplot on the right of the month segment. MLP predicted results are shown using the solid lines. Concentration in mixing ratio.

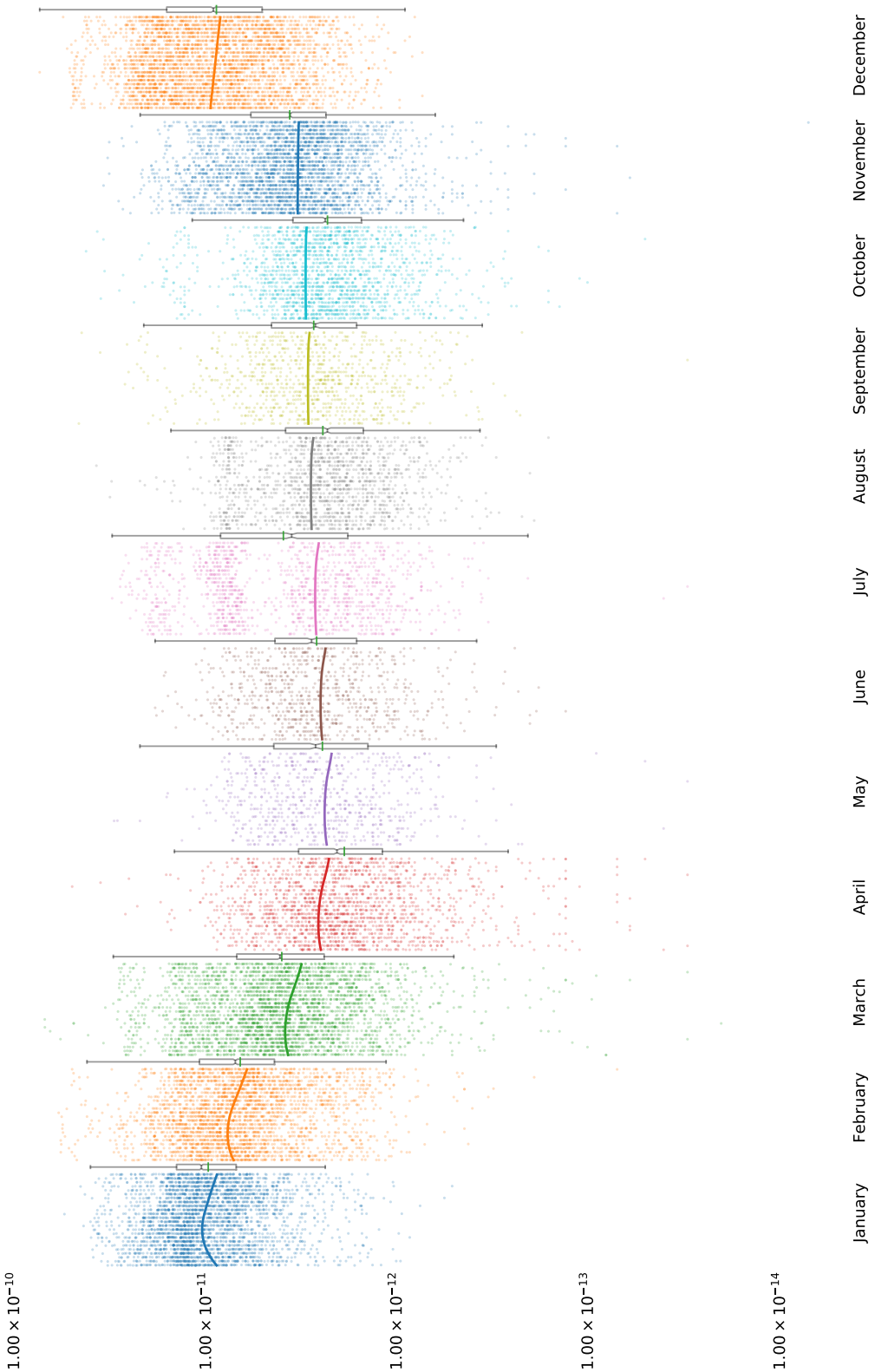

Figure 1.23: **Cape Verde MLP predicted and observational data of iso-Pentane.** Each segment represents data from a different month. Within each month segment exists 24 hour segments to create a diurnal. Observational concentrations are plotted in the form of a translucent scatterplot and summarised using the boxplot on the right of the month segment. MLP predicted results are shown using the solid lines. Concentration in mixing ratio.

1.6.1.4 Model Initialisation Procedure

The aim is to generate a set of initiation concentrations which are representative of the different types of chemistry between environments. In this section, we are not interested in the exact concentration modelling for specific times or scenarios. Instead, we seek to generate representative of the processed chemistry under a range of conditions.

To do this species concentrations are extracted from an MLP regressor trained on observational data for each scenario. Each concentration is that of noon local time from the generated diurnal from summer observations at each location. This produces a monthly error of $\pm 2 months$ from June. As both nitrogen oxide and dioxide are supplied the total NO_x for each simulation are *not* constrained. The initial conditions are shown in Table 1.4.

In general observational measurements are not able to detect all the species presented within the MCM. This means that to be able to compare model scenarios, the chemistry must first be spun up. In propagating the chemistry forwards in time, primarily emitted and measured species are broken up forming the intermediate species which exist within a mechanism. To reach a steady-state, the model is initiated at noon and the observational concentrations are rest every 24 hours. For each diurnal, the fractional difference between the concentrations at each day are compared. If the difference between these is less than 0.001, the model is left to run unconstrained for 5 days (right of the dashed line in Figure 1.24-1.27). Model results are then taken after 3 days of unconstrained runs. The reason for this is that the total RO_2 concentration takes longer to stabilise in the polluted environments (London and Beijing). This falls into a periodic cycle beginning noon on the third day and can provide a representation of the processed chemistry within each environment.

NOTE: It should be noted that some of the concentration plots may appear to lose their diurnal dependability. This may be attributed to the changing order of magnitude of the concentrations, and that the species are still responding as expected.

1.6.1.5 Extracting the required results

Model diagnostics such as concentration and the net flux passing through a species may be extracted directly from the DSMACC box model. These provide the baseline comparison and can be directly compared to the graph metrics. Species concentration tells us the abundance of different species, and the net-flux tells us how fast this is changing in time.

As some species may have a fast inwards and outwards flux (low net-flux), the absolute flux is also included. Finally, the sensitivity of each species for other species is also extracted (the jacobian matrix). This serves to not only generate the graph used to represent the chemistry, (subsection 1.5.1)

but also to identify the overall influence a species has on others in the network. This can be calculated by taking the net sum of the influence a species has on every other from the Jacobian. This is analogous to calculating the outdegree of a node in the jacobian network.

Species	Beijing(APHH)	Borneo(OP3)	London(ClearFlo)	CapeVerde
LAT	39.9	0.96	51.0	16.5
LON	116.3	114.5	0.00	23.4
O_3	6.883e-08	8.939e-09	3.819e-08	2.629e-11
NO	1.660e-09	2.668e-14	2.350e-09	2.358e-12
NO_2	1.226e-08	1.081e-13	7.445e-09	8.447e-12
HCHO	4.472e-09		1.119e-08	
C_2H_6	3.163e-09	7.315e-10	2.133e-09	4.539e-10
C_2H_4	1.004e-09	1.152e-10	4.893e-10	2.481e-11
C_3H_8	3.019e-09	1.924e-10	1.128e-09	1.728e-11
C_3H_6	1.335e-10	1.333e-11	1.784e-10	9.343e-12
IC_4H_{10}	6.412e-10	8.742e-11	5.142e-10	2.486e-12
NC_4H_{10}	1.593e-09	5.698e-11	1.058e-09	4.481e-12
C_2H_2	1.058e-09	1.825e-10	3.018e-10	1.848e-11
TBUT2ENE	4.198e-11		1.815e-11	
CBUT2ENE	4.454e-11		1.305e-11	
IC_5H_{12}	1.047e-09	2.883e-11	7.424e-10	3.470e-12
NC_5H_{12}	4.650e-10	2.090e-11	2.792e-10	2.513e-12
TPENT2ENE	3.939e-11			
CPENT2ENE	3.982e-11			
NC_6H_{14}	2.057e-10	6.437e-12	6.357e-11	
C_5H_8	7.134e-10	1.957e-09	1.640e-10	
NC_7H_{16}	7.905e-11		5.222e-11	
BENZENE	4.045e-10		1.137e-10	7.682e-12
NC_8H_{18}	3.091e-11		1.442e-11	
TOLUENE	6.767e-10		3.205e-10	3.121e-12
EBENZ	3.115e-10		6.017e-11	
OXYL	1.677e-10		5.049e-11	
CH_3CHO	4.783e-10		4.095e-09	
C_2H_5OH	4.655e-09		3.125e-09	
CH_3COCH_3	3.328e-09		2.924e-09	
NC_9H_{20}	1.336e-11		7.922e-11	
$NC_{10}H_{22}$	1.062e-12		1.602e-10	
α-PINENE[17]	7.341e-11	15e-11	1.105e-10	
LIMONENE	5.836e-11	1.351e-10	3.566e-11	
$PXYL^+MXYL$[18]	4.943e-10			
IPBENZ	4.567e-10			
PBENZ	3.996e-10			
HONO	6.479e-10		4.109e-10	
MACR		6.948e-11	1.862e-11	
$PENT_1ENE$			2.383e-11	
MVK			2.091e-11	
NPROPOL			2.883e-10	
NBUTOL			4.535e-10	
STYRENE			2.241e-11	
MEK			5.494e-11	
C_3H_7CHO			9.534e-12	
C_4H_9CHO			1.865e-11	
$C_5H_{11}CHO$			1.201e-11	
CYHEXONE			9.790e-12	
BENZAL			1.510e-11	
PAN			1.791e-10	

Table 1.4: The initial conditions created from the MLPRegressor prediction of observational data. Although not specified the concentration for methane is set by the model at 1770ppb.

[18]This is written as ?-pinene in the merged CEDA dataset for the Borneo OP3 campaign. This is due to character conversion errors.

[18]The concentration for these is split evenly between both species

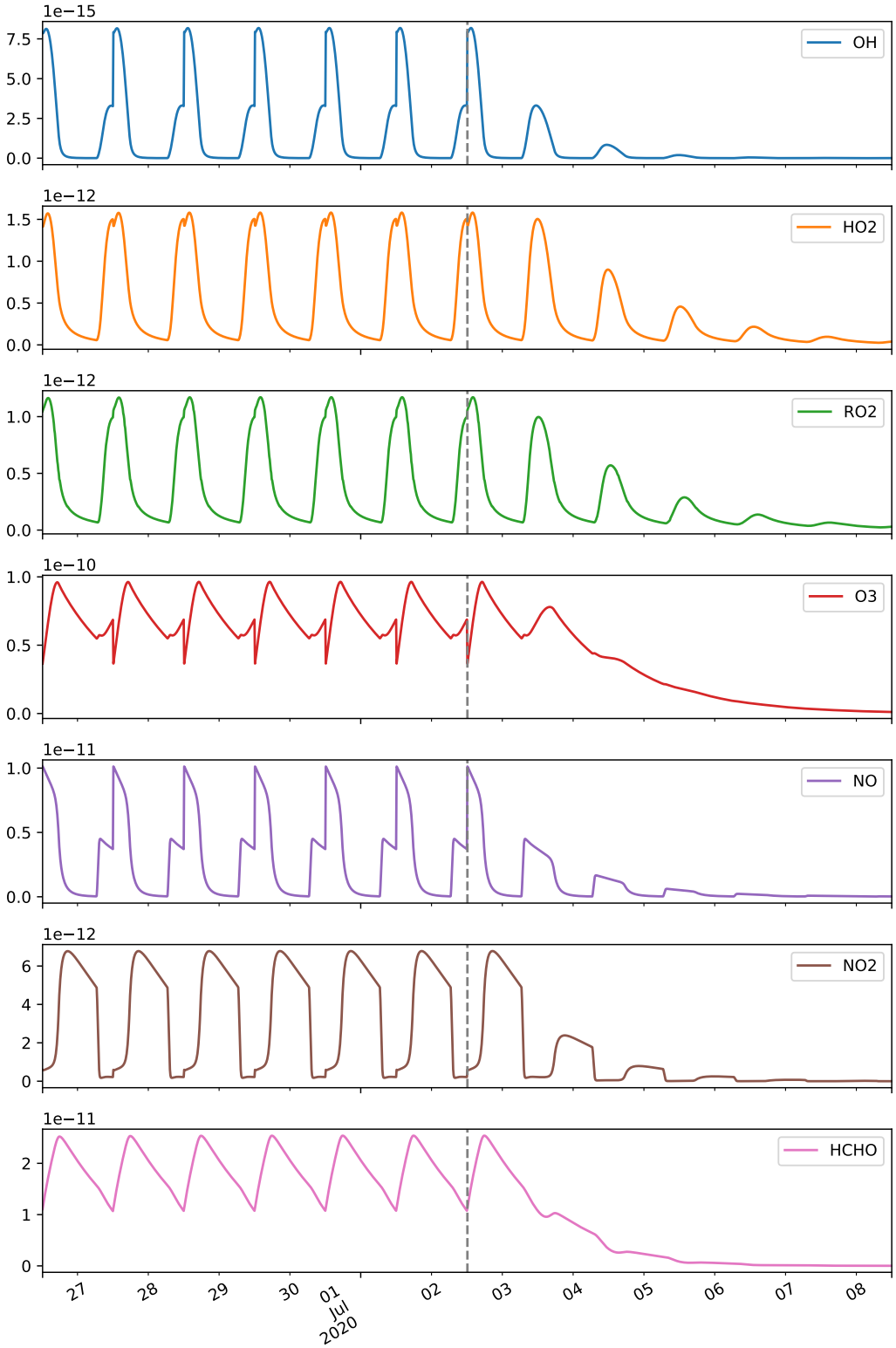

Figure 1.24: **The concentration profile for CapeVerde.**This shows a the change in concentration over time for HO_x,NO_x,Ozone and RO_2 species for a simulation run generated by the mlpregressor. Left of the dashed line shows the last 6 days of spinup, where the intial concentrations are reset at noon each day until the species fractional difference is less than 0.001 .

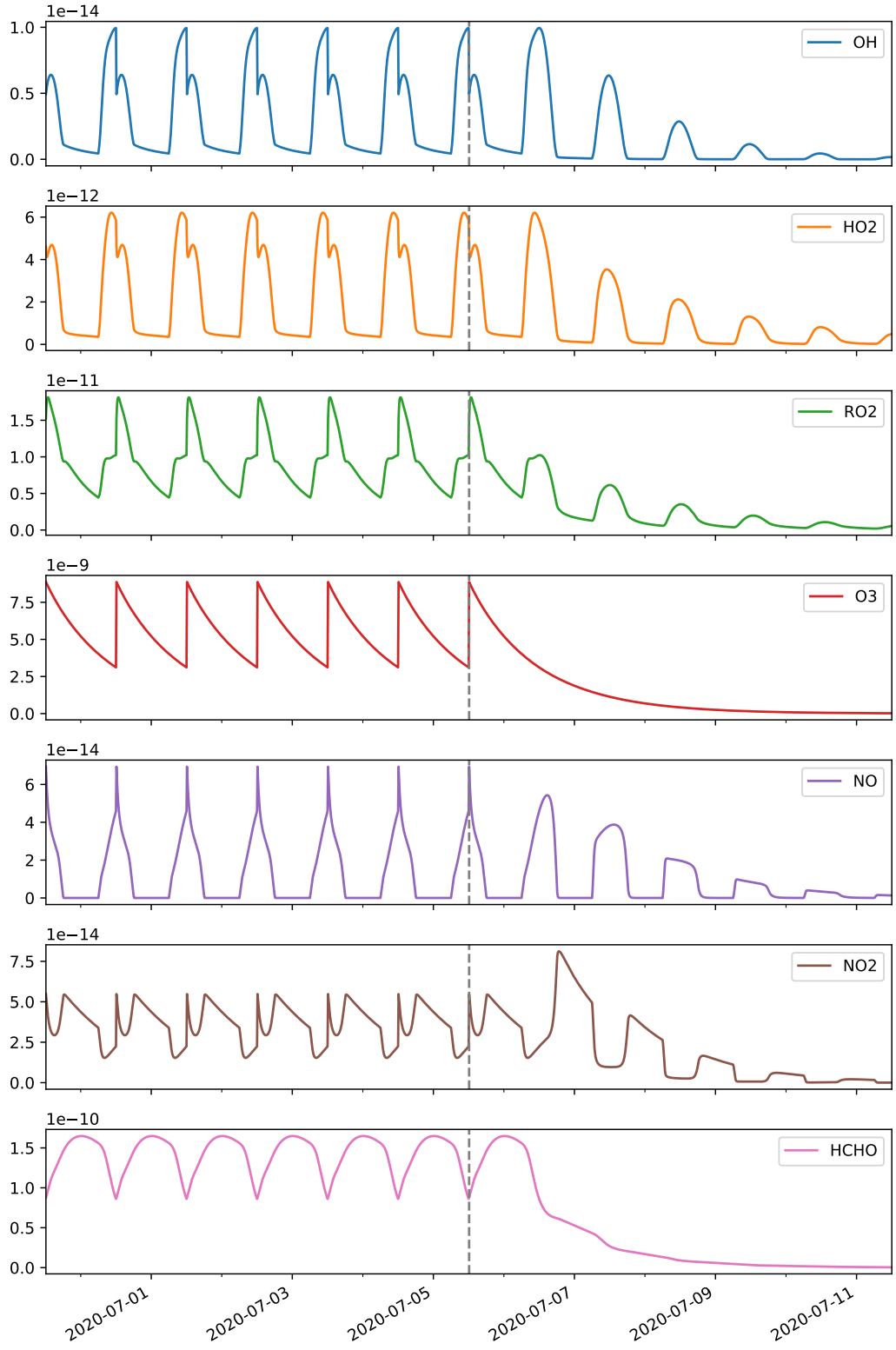

Figure 1.25: **The concentration profile for Borneo.**This shows a the change in concentration over time for HO_x, NO_x, Ozone and RO_2 species for a simulation run generated by the MLPRegressor. Left of the dashed line shows the last 6 days of spinup, where the initial concentrations are reset at noon each day until the species fractional difference is less than 0.001 .

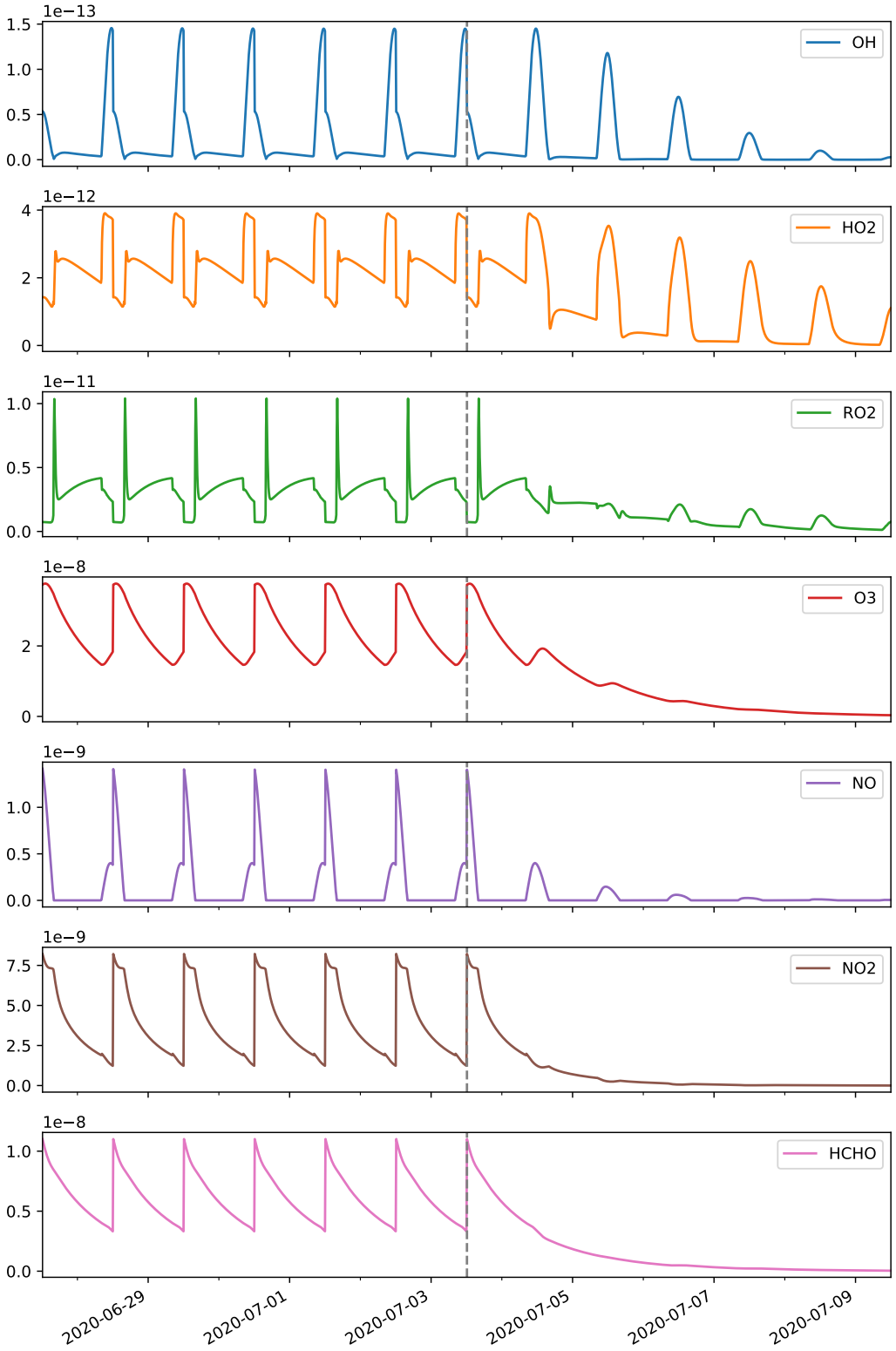

Figure 1.26: **The concentration profile for London.**This shows a the change in concentration over time for HO_x,NO_x,Ozone and RO_2 species for a simulation run generated by the mlpregressor. Left of the dashed line shows the last 6 days of spinup, where the intial concentrations are reset at noon each day until the species fractional difference is less than 0.001 .

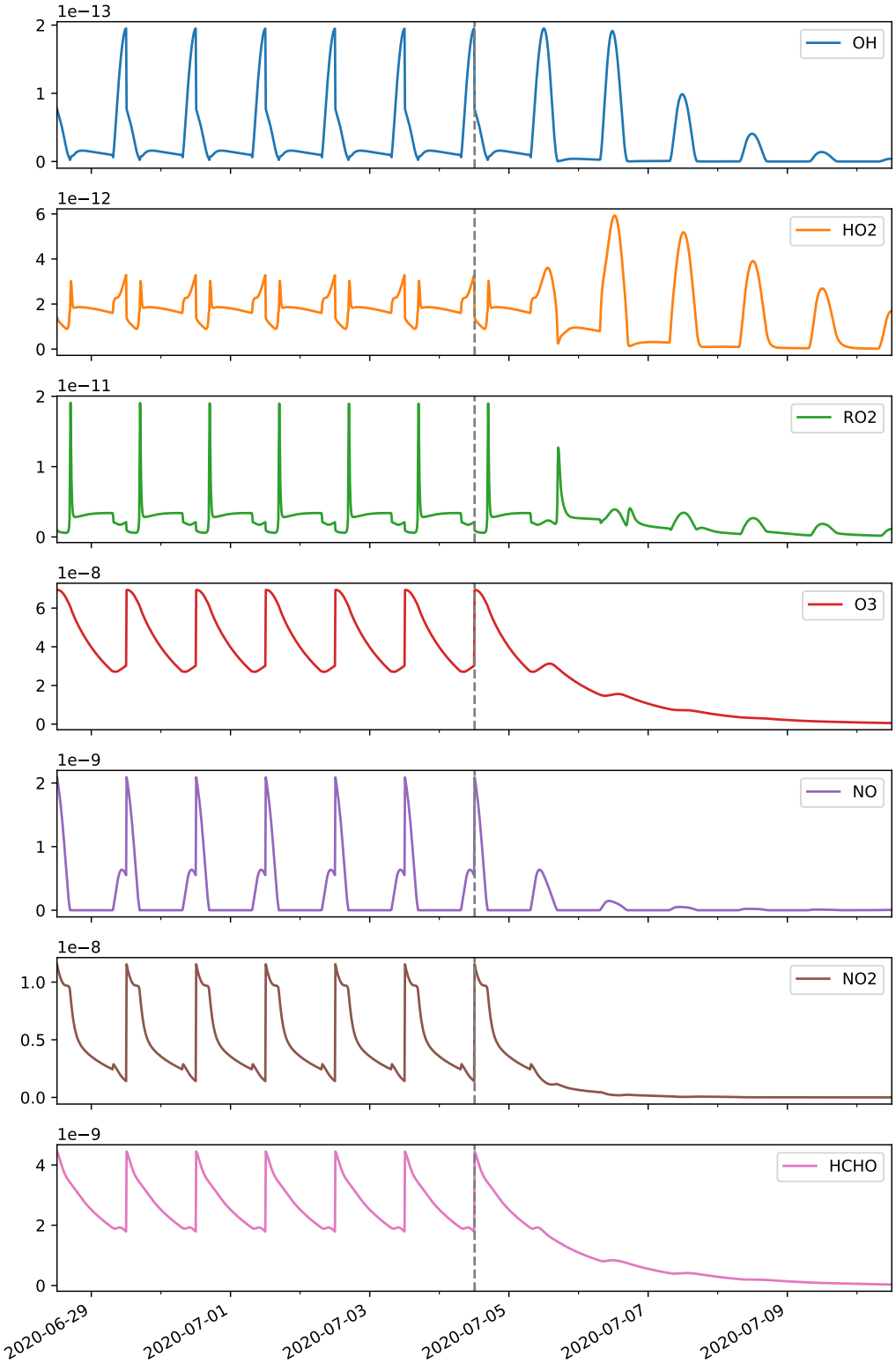

Figure 1.27: **The concentration profile for Beijing.**This shows a the change in concentration over time for HO_x, NO_x, Ozone and RO_2 species for a simulation run generated by the MLPRegressor. Left of the dashed line shows the last 6 days of spinup, where the initial concentrations are reset at noon each day until the species fractional difference is less than 0.001 .

1.6.1.6 Unifying the results

Each metric provides a different range in which it ranks the importance of a node. To account for this all results are scaled to the range {0,1}, where 1 is the highest. Entries, where the results span several orders of magnitude (e.g. concentration, flux, influence), are flattened using the $\log_{10}$ scale before being normalised.

1.6.2 Comparing Results

This subsection juxtaposes the use of traditional model diagnostic methods against a selection of graph metrics. As there are several thousand species within each simulation run, the keyword extraction algorithm Term Frequency - Inverse Document Frequency (TF-IDF), is used to identify the top most prominent species for each metric (traditional and graph). From this, the 10 highest-ranking species from each category are collated into a single diagram for comparison.

1.6.2.1 What is TF-IDF

TF-IDF is a numerical statistic used in text natural language processing and text mining. It is designed to identify the importance of a word concerning its context.

It provides a value for the frequency a word appears within a document, offset by the number of times it appears in other documents within the corpus - It is for this reason that 83% of text recommender systems in digital libraries use TF-IDF, [Beel et al., 2016].

In [Ellis, 2019] I applied this to the chapters of Frankenstein and found the keywords extracted almost exactly replicated those from the synoptic description of the novel. Although TF-IDF is a text mining procedure, the algorithm itself is mathematical, meaning that it may be applied to our diagnostic dataset. The working of the algorithm is discussed below.

Term Frequency

The TF from the algorithm name stands for term frequency. This is an analysis of the number of times a word exists within a dataset. There are several ways in which this can be done, these are:

- **Raw Count** - The *number of times* a word exists within the document.
- **Boolean/Logistic** - $True$ if the word exists, false otherwise.
- **Adjusted for Document Length** - $word\ frequency/total\ number\ of\ words$

- **Log Scaled** - $\log(1 + frequency)$

As the scaled values for each item are taken, we can liken our results to the 'Adjusted for Document length' equation and use the scaled ranking value for each group respectively.

Inverse Document Frequency

Inverse document frequency tells us how much information a word provides concerning a certain context. Whilst a word may be used extensively throughout the corpus (i.e. term frequency) it is often that we are interested in words which are only frequent within a specific document. This is one of the reasons TF-IDF is useful in the extraction of keywords from a document.

The inverse frequency of a word is usually calculated as the log of the fraction of documents N against the number of documents the word appears in D_f, Equation 1.14.

$$IDF = \log(\frac{N}{D_f}) \tag{1.14}$$

If required, changes can be made to produce results which show a better representation of words which are important for all documents (probabilistic, Equation 1.15) or individually (smooth, Equation 1.16). However in looking at Figure 1.28, it can be seen that the basic IDF formula mentioned has a limit of zero the greater the document frequency (D_f), which makes it easy to normalise against - i.e. divide by 2 as this is the value tended to if the document frequency tends to 0.

$$IDF_{prob} = \log(\frac{N - D_f}{D_f}) \tag{1.15}$$

$$IDF_{smooth} = \log(\frac{N}{1 + D_f}) + 1 \tag{1.16}$$

To complete the TF-IDF equation, the term frequency and inverse document frequency terms are multiplied together.

Applying TF-IDF to chemical metrics

To identify metrics selection criteria, we seek only species which are important only in that category. To do this the TF-IDF algorithm can be adapted for use with the graph metric output. Here 'Term Frequency' corresponds to the number of times a value appears within the body of a document and

can be seen as the scaled {0,1} metric output. This is then divided by the log of the 'Inverse Document Frequency' with D_f being the sum of values across all the metrics. This makes the TF-IDF equation:

$$TF.IDF = metric\_value\ .\ \log(\frac{N_o\ documents}{\Sigma_\forall\ metric\_values}) \tag{1.17}$$

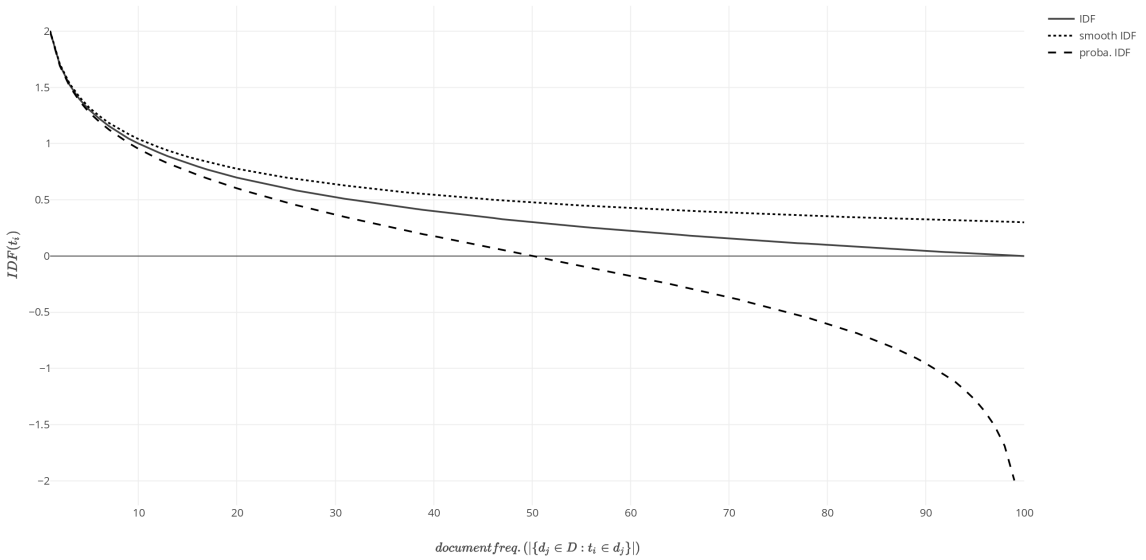

Figure 1.28: **The different IDF outputs.** A plot showing Inverse Document Frequency profiles against Document Frequency. This shows that the probabilistic IDF highlights words that are more important across all items, whilst the smooth IDF shows files which are more important individually. The general IDF (which is used) produces a result starting at 2 and tending to zero. This provides the best response and can easily be scaled between the range of [0,1] by dividing the output by 2. Source: [Mquantin, 2020]

1.6.2.2 Metric Comparison

This section aims to compare the efficiency of graph metrics against a list of traditional methods. To do this the use of a bivariate colourmap (Figure 1.29) is used. Each figure consists of a red-hued image/heatmap representing the scaled values {0,1}:{white, red} for each of the individual columns. As each simulation contains thousands of species, only the top 10 species from each column/category are selected. These are then sorted by the average sum of their closeness, betweenness and page-rank values (blue column). Superimposed on this reds-only heatmap is a blue heatmap representing the average sum of the three metrics for comparison. Such a method allows for the comparison of individual values against an approximation of species importance, by the sum of graph metrics - allowing an easy categorisation of the data:

- **Purple** - This value is high in both the individual category and the metric sum.

- **Red** - This value is high for the individual category but not the metric sum.

- **Blue** - This value is high for the metric sum but not the individual category.

- **White** - This value is low for all categories.

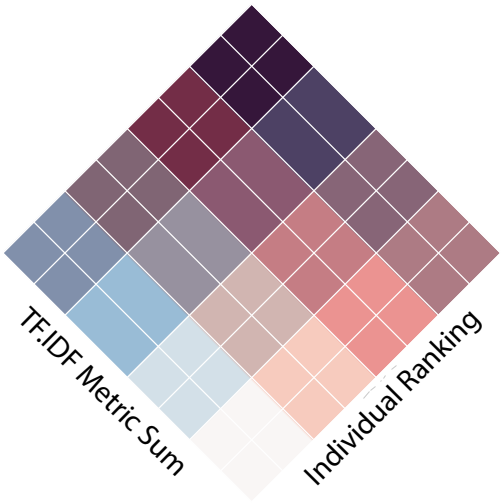

Figure 1.29: **The bivariate colourplot key.**

1.6.2.3 Individual Categories

Individual categories are split between traditional metrics and graph centrality metrics. To represent the importance of a species the following values may be extracted through the use of a simple box model:

- **Concentration** - This describes the abundance of a species within the atmosphere.

- **Net Flux** - This describes the rate of net (absolute) change of concentration over time for a species.

- **Absolute Flux** - Some species may have a large flux going through them (production and loss), resulting in a small net flux. This sums the production and loss fluxes.

- **Influence** - Influence is the total magnitude of an effect that changing a species concentration by 1% would have on other species within the network. Since the graph is generated using the Jacobian matrix, an alternative method for calculating this can be by calculating the total out-degree of a node.

The importance of a species is then compared through the use of three of the most common centrality metrics. These are:

- **Centrality** - This describes how easily information from one node can be disseminated to all other nodes.
- **Betweenness** - This describes the number of shortest paths (fastest fluxes/greatest influences) that are routed between nodes adjacent to our chosen node. Species with a high betweenness hold a brokering position and can act as a bottleneck between different groups of chemistry.
- **PageRank** - PageRank looks at the flow in a system. It ranks nodes not only on the number of species it reacts with but also the importance of the species it has reacted with.

Finally, the 'Metric Sum' is the sum of all the metric values scaled between 1 and zero (the mean).

1.6.3 Senario Analysis

In selecting the top 10 ranking species for each category it is possible to examine if the importance of a species with centrality metrics varies from the results suggested by traditional metrics. In this subsection, we explore the TF-IDF rankings of each metric and use this to decide if species importance is local to a specific metric. We look at what species are highlighted by each scenario and compare them against the primary emitted species shown in Table 1.4. Finally, we compare the total metric sum against the traditional metrics of concentration and flux and compare the correlation.

Cape Verde

The initial conditions for Cape Verde have low levels of NO_x and ozone. The chemistry is split between aromatics and small alkanes. The aromatic species are of a similar magnitude to the alkanes. Many of the aromatic products are shown to be important in Figure 1.31, which may be due to the larger aromatic species <break down?> potential (they have more carbons to form bonds with). Using this it can be seen that many of the species highlighted are products of Toluene, Benzene, Phenol and Catechol (the latter of which are produced by adding an alcohol group to a Benzene ring - Figure 1.30). These are most likely emitted either from mainland Africa or through ship emissions and are important indicators of how processed the chemistry of the atmosphere is. Benzene and Toluene are usually emitted at a ratio of 1:4 respectively and the same rate. Since Toluene reacts at a much faster rate, a change to this ratio allows tells us how much the chemistry within a system has changed. It may be suggested both from the initial conditions and the metrics that the chemistry is one which has been transported to the island, rather than emitted there. In addition to the aromatics, many of

the primary emitted alkanes, and their products, have been highlighted. These tend to be unreactive (and thus long-lived) which can be seen by their low betweenness[19] values - they are unlikely to act as a fast-reacting proxy between two other species. The change in colour between the metrics suggests that for the Cape Verde Mechanism important species are not often central (easy to get to - closeness centrality) from all other species. The selected species ranking the highest closeness (Propane-Pentane) do not seem to be ranked important as part of betweenness or page rank which results in the red colour for the plot (low overall metric sum). Species ranked high by the PageRank algorithm do not have a high betweenness or net flux value, but do have large absolute flux. This suggests that although they may not have the fastest fluxes going through them (low betweenness), they act as an intermediate reaction for other chemistry where they are produced and lost at a similar rate (low net flux, high absolute flux.).

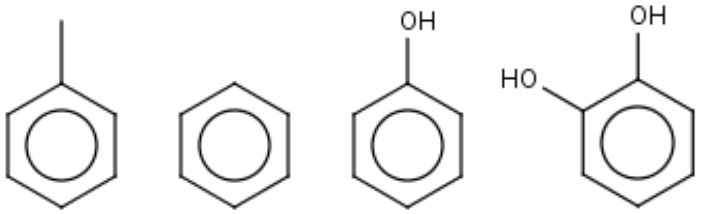

(a) Toluene (b) Benzene (c) Phenol (d) Catechol

Figure 1.30: **Chemical structures of the 4 most common type of aromatic species in cape verde.**

Borneo

The Borneo dataset, through the nature of being located in a rainforest, contains no benzene ring based aromatics. From its initial conditions the simulation begins with a higher level of Ozone, High Isoprene (C_5H_8), and moderate amounts of Acetylene (C_2H_2), α-pinene, and limonene (both ($C_{10}H_{16}$)). Figure 1.32 shows a very large of the rainforest chemistry is dominated by terpenes (mainly Isoprene) products. Unlike Cape Verde, these all have a high concentration, net-flux and absolute flux. This suggests that the products act as intermediate species for the chemistry and are both produced and lost at a high rate. Much of these species have a high closeness and a high page rank, suggesting that the centre of the Borneo network is very close-knit, and the well connected to species of importance. The only outlier to this is $CISOPAO_2$ which is has fast reactions flowing through it and has important connections (it is only a couple of steps away from Isoprene) but does not have a high closeness centrality. This suggests that it is located as part of a terpene branch but not at a highly pivotal position. The uniformly distributed colour gradient for betweenness suggests

[19]Most of the species with low betweenness values are a product of Ethane (C_2H_6), Propane (C_3H_8), Butane (C_4H_8) and Pentane (C_5H_{12})

that there are many possible reaction routes a species may undergo before being converted into carbon dioxide and water. The exception to this is $C_{517}CHO$ which has 14 precursors and only 2 products (a bottleneck / pivotal position), resulting in the highest betweenness value of the network.

London

The London dataset contains a mix of anthropogenic and biogenic aromatics and long-chain alkanes. Similar to Cape Verde we have a section of alkanes which have a low overall metric sum, with a small value for closeness and page rank. Combined with their high net flux, absolute flux and influence values, this suggests that they have a moderate directional flux, most likely influencing the production of many other species at a consistent rate. In addition to these, we have species with a moderate closeness but a high betweenness. These are often species such as formaldehyde (HCHO), glyoxal (C_2O_2) and acetaldehyde (CH_3CO_3) which can serve as tracers for fast photolytic reactions. This is because on the graph structure (**??**) they sit between the dense centre of the network (high closeness) and the branches formed from each primary emitted species (low closeness). Their high connection density and importance in the network is also picked up by the page rank algorithm. Other species with high betweenness and a low centrality are the monoterpenes limonene and α pinene, as well as hexane (NC_6H_{14}) and butane products. These are (or are close to) primary emitted species and therefore have a low closeness. Since this also means that much of the chemistry originates with them, the outward 'flow' of information also results in a lower page rank value.

Beijing

Similar to London, the fast photochemical tracers are identified, although some have a slightly lower flux between them (betweenness) and page rank values. This suggests that the network structure or weightings may have shifted slightly, creating more links, or importance in a specific branch of chemistry. Additionally, their overall metric sum is lower. Glyoxal, Methyl Vinyl Ketone (MVK) and their associated criegee configurations all feature heavily in the middle of Figure 1.34. These are important as they represent the fast chemistry formed by both the anthropogenic and biogenic chemistry that is within the simulation. These tend to have a high closeness and page rank centrality, a pattern that is also seen with the long-chain alkane products from Octane (NC_8H_{18}), Hexane (NC_6H_{14}) and isoprene.

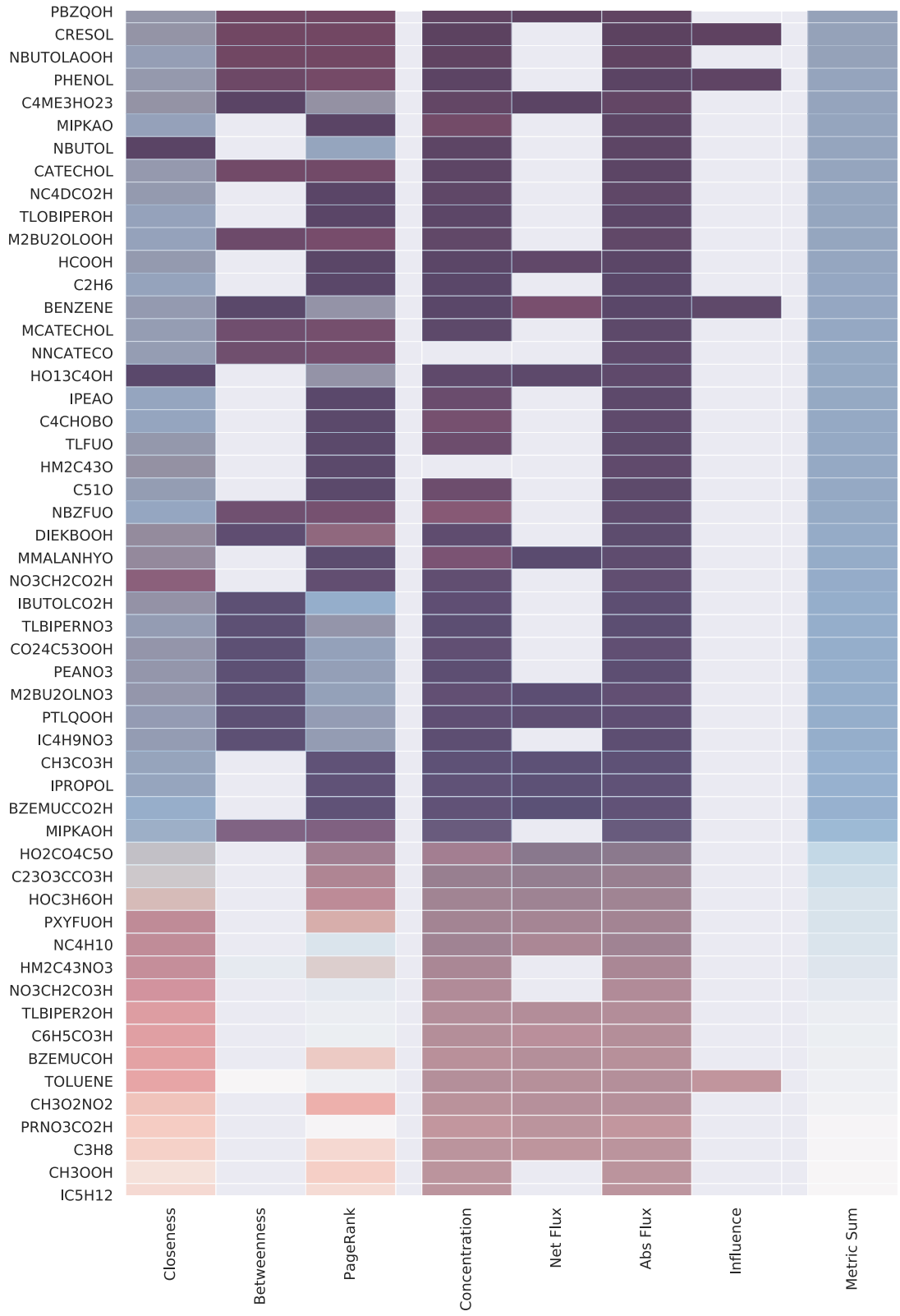

Figure 1.31: **A bivariate heatmap comparison of Cape Verde.**

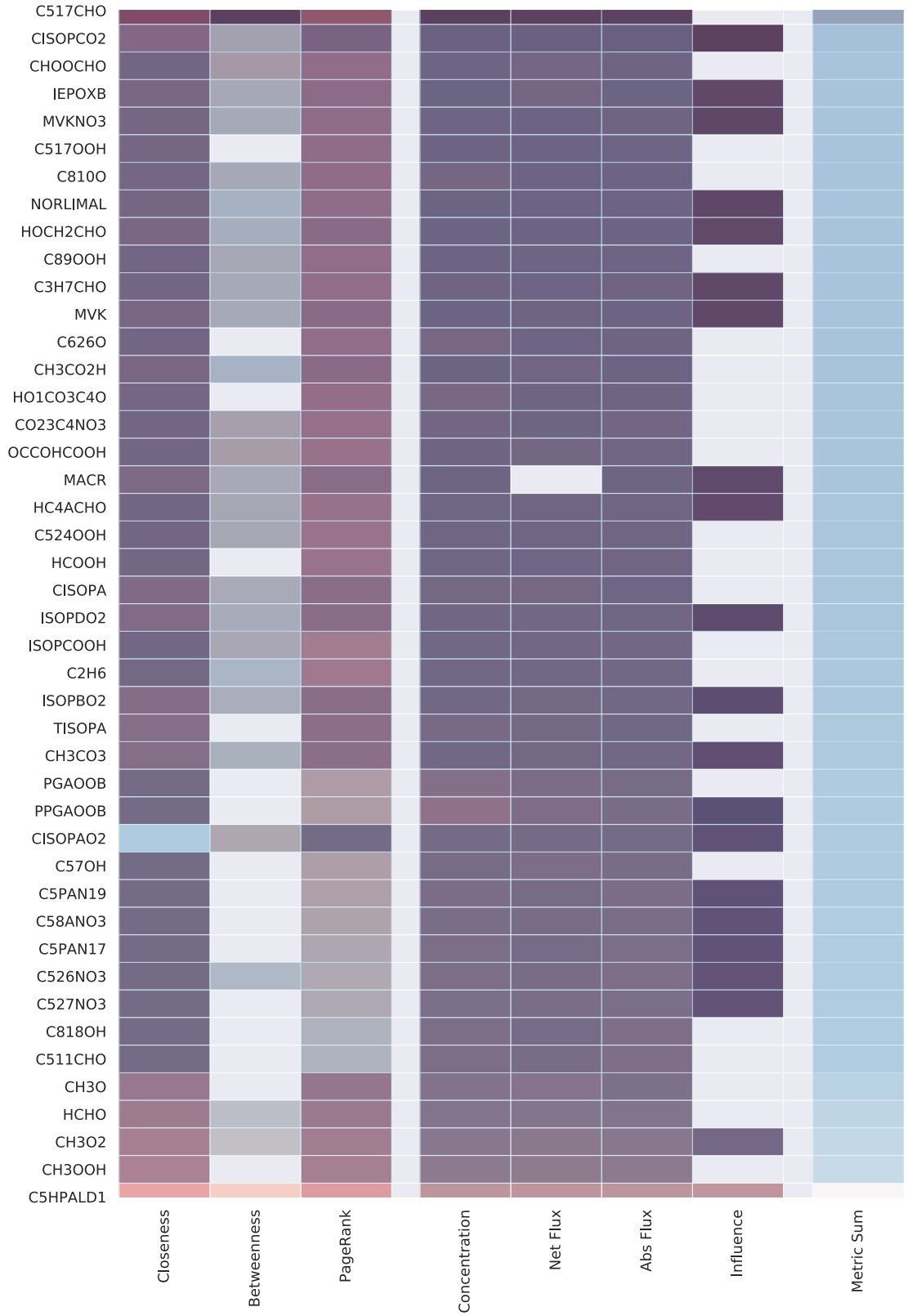

Figure 1.32: **A bivariate heatmap comparison of Borneo.**

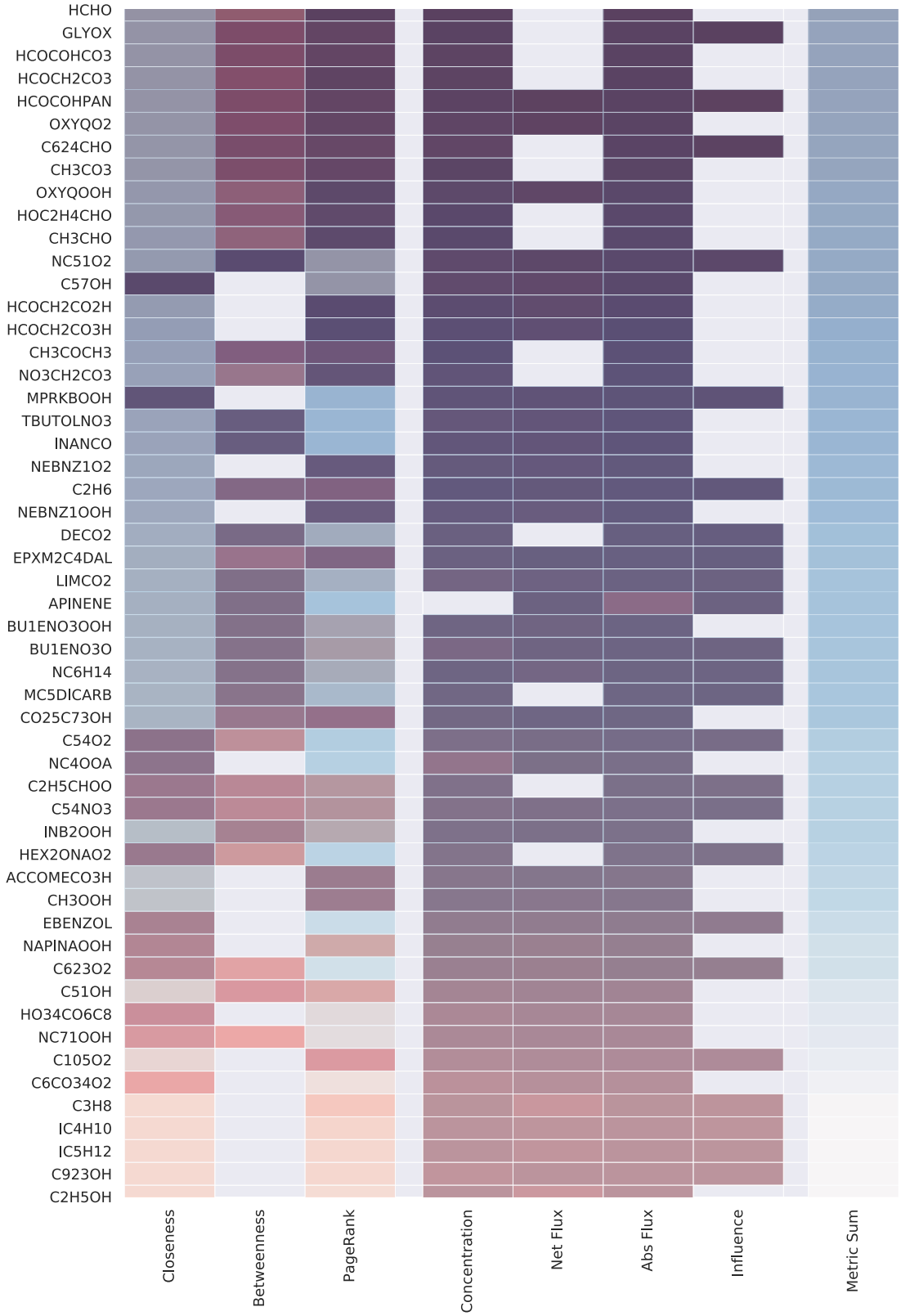

Figure 1.33: **A bivariate heatmap comparison of London.**

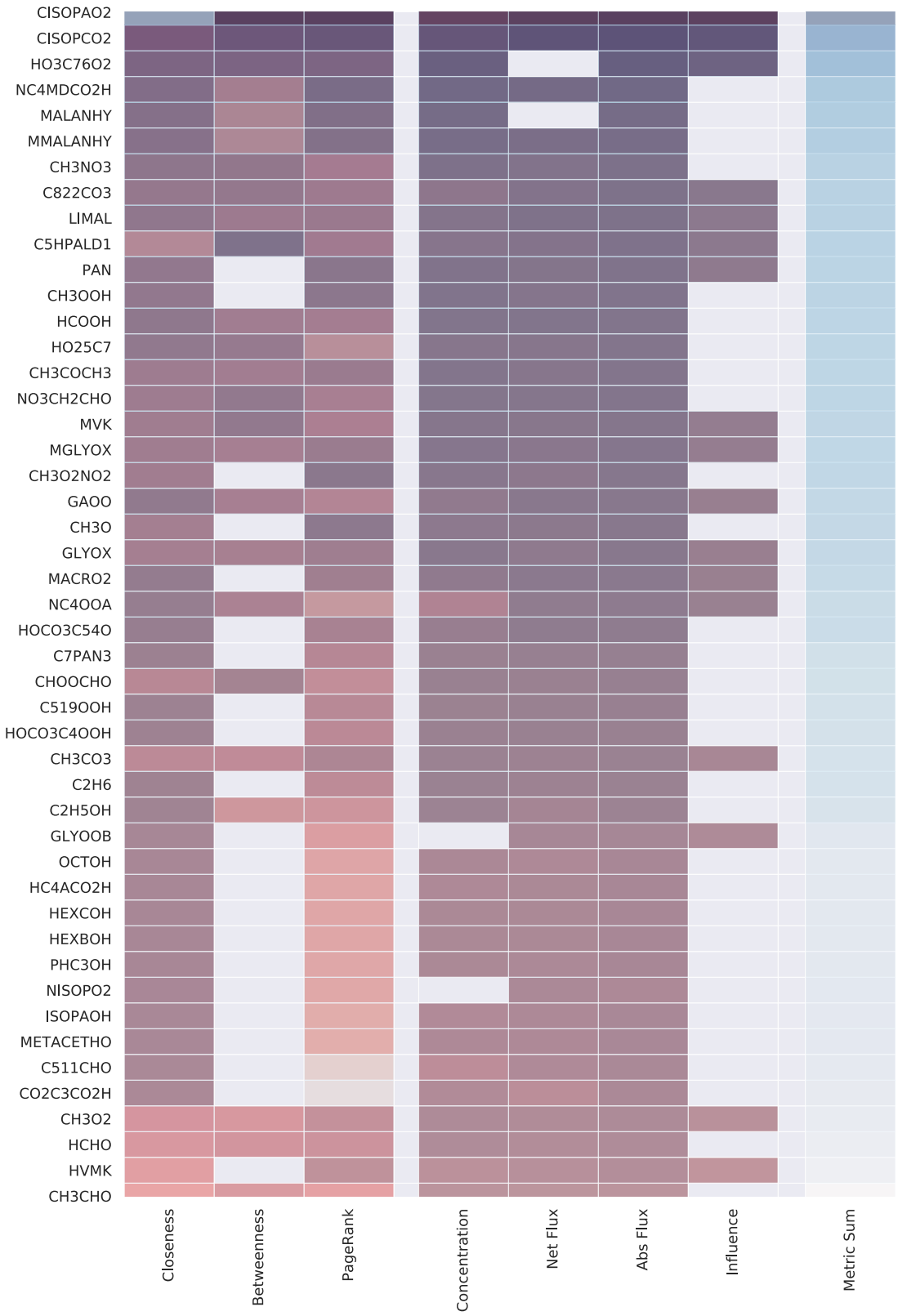

Figure 1.34: **A bivariate heatmap comparison of Beijing.**

Ability to match traditional metrics

All graph construction Colours - all purple, suggests a general agreement photochemical tracers

1.6.4 Providing an overall overview using the TF-IDF and the metric sum.

In the previous section, it was shown that centrality metrics can be used to complement the use of traditional metrics in the analysis of the chemical network. As each metric represents a different aspect of importance, should a single ranking value for a node be required, it is possible to take the average sum of all three metric values. Looking at Figure 1.31-1.34 it is possible to see similar trends in colour gradient between the purples of the traditional metrics of flux and concentration with the total metric sum (the blue column). This suggests that it is possible to compare each scenario with the use of the metric sum.

In selecting the ten highest-ranking species from the mean centrality metric table for each simulation, Table 1.5 can be created. Unlike the previous method, we are now looking at species which are important across all metrics in a simulation. For Borneo species produced from Heptane, Hexane, Isoprene and Limonene are seen as important. Cape Verde, similar to before, has a selection of Benzine related products such as Phenolic and Catecholic compounds. Beijing consists mainly of Quinones and Dialdehydes which are both derivatives of Benzene. London again has Benzine related compounds, mixed with the fast photochemical indicators, which were also ranked highly in Figure 1.33. Looking at the highest-ranking sum (Nan-mean), it is seen that isoprene, hept/hexane and glyoxal products highlighted as the most consistently important across all four simulations.

	London	Cape Verde	Beijing	Borneo	Nan-Mean
0	HCHO	PBZQOH	PTLQONE	C622OH	CISOPCO2
1	CH3CHO	PHENOL	PBZQONE	C923OH	CISOPAO2
2	C5CO14OOH	C24O3CCO2H	HOHOC4DIAL	C54OH	C517CHO
3	PBZQOOH	NBZFUONE	MNNCATCOOH	HO2C4OH	HO2C6O2
4	MALANHY	TLBIPERNO3	C6H5CO3H	C624OH	HCOCH2CO3
5	CH3CO3	BZBIPERO	EPXDLPAN	HEXAOH	C717O2
6	C57OH	TLEMUCCO2H	C5DIALO	C822CO2H	HCOCOHCO3
7	C624CHO	BZEMUCCO2H	NBZFUOOH	MACROHOOH	HOCH2CH2O2
8	GLYOX	PTLQO	TLBIPEROOH	HO14CO2C4	HOC2H4CHO
9	HCOCOHCO3	NNCATECO	NCRESOOH	C624CO2H	C626CHO

Table 1.5: **A table of the top 10 ranked species for each simulation.** Only species that exist within atleast 3 out of the 4 simulation are used. The Nan-Mean takes the mean of all available data, ignoring runs where a species is not present.

A note on finding the precursors

Graphs are also useful in the back navigation of a network. It is possible to discover the most probable primary emitted species (nodes with no in-degree) by comparing the shortest path lengths for all primary

emitted species (not including inorganic species). Here the primary emitted species with the smallest number of connections are often the most likely source.

1.7 Calculating production sensitivity using personalised page rank.

In the calculation of the PageRank result by solving for the eigenvalues and vectors of the google matrix was discussed. It was also mentioned that an equivalent method to get a result may be obtained by propagating the one's vector in small increments, 2. This works much like the integrator within a chemical box model, except rather than updating the species concentration with each time step, we move information between each node.

Using this analogy it, therefore, follows that should we reverse the direction of the flow (change the edges from source $\rightarrow$ target to source $\leftarrow$) it would be possible to see where species influence originates, Figure 1.35. As each network is constructed directly from the Jacobian matrix (what is used within the integrator to propagate a model forwards in time), reversing the link direction is analogous to taking the transpose of the jacobian. Within the modelling world, the resultant matrix is now known as the adjoint. The adjoint matrix is often used in the running of models backwards in time, to make historic predictions based on current data.

Some information on using the adjoint and references here

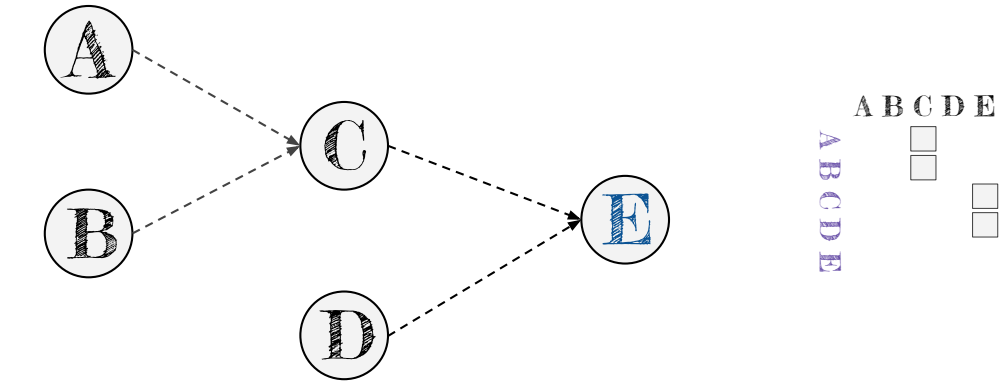

(a) Traditional Influence Graph

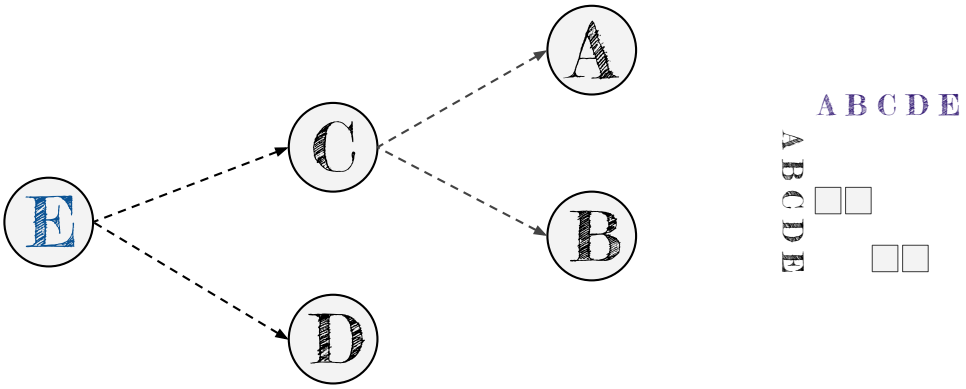

(b) Reversed-link (adjoint) influence graph

Figure 1.35: **Link reversal of the Jacobian Sensitivity matrix graph results in a graph of the Adjoint.** Showing how in changing the direction of the links in a graph is equivalent to applying the transpose to an adjacency matrix (right). In the case of a Jacobian based graph, this is analogous to using the adjoint to propagate the model back in time - something that can be used to identify the influence upon a species with a model.

1.7.1 Testing

As with all scientific processes, it is important to first test the algorithm on a small, comprehensible example. To do this we start with the creation of CH_2OO within the Borneo mechanism. This is a direct product of isoprene. In tracing back all the species precursors the mechanism for its creation can be described as:

$$O_3 + C_5H_8 \xrightarrow{\kappa} CH_2OOE + (MACR\ or\ MVK) \tag{1.18}$$

$$CH_2OOE \xrightarrow{\kappa_{\mathrm{dec}}} CH_2OO \tag{1.19}$$

In traversing the adjoint/reversed graph, this presents a singe 'shortest path' between the product and its precursor. This creates a base test for the algorithm. The PageRank algorithm is now run

with a personalisation vector consisting of a value of 1000000 for the species of interest and -1 for all others. A damping factor value of 0.01 is also used for the algorithm.

As CH_2OOE only has one precursor (α-pinene) the initial test is done on this. From this, the identification of isoprene as a source is successful, although since the algorithm is performed on the whole network, there are results for several additional species, Table 1.6. This is because page rank works on using teleportation to change between items in the evolution of the system. With the design of the personalisation vector, these values will, however, be significantly smaller than any containing useful results.

C_5H_8	9.920000e-03
CH_2OOE	9.920000e-01
$C_{816}O$	-9.990000e-07
$NC_{101}CO$	-9.990000e-07
$C_{926}OH$	-9.990000e-07

Table 1.6: A reversed graph Page Rank test with $C_5H_8 + O_3 \longrightarrow CH_2OOE$ as the only reaction.

Next, we apply the same methodology to CH_2OO. This creates the graph in Figure 1.36. Here it is seen that CH_2OO is directly dependant on the radicals $CH_2OO[F, B, C, G, A]$, and CH_2OOE. This is then dependant on Isoprene, which then has a range of dependencies with all have precursors of their own (not shown). Table 1.8 shows the direct dependence on Isoprene and the criegee radicals of CH_2OO in addition to

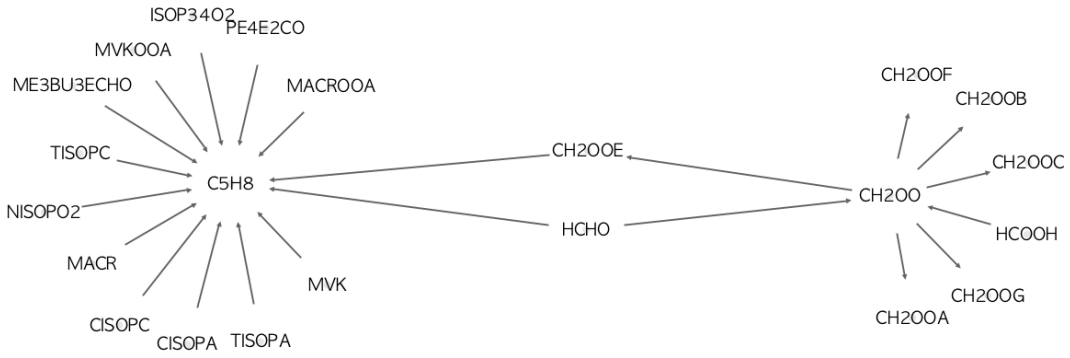

Figure 1.36: **The reversed subgraph between Isoprene, CH_2OOE and CH_2OO.** This is a subgraph of the afforementioned species, showing them and their neighbours. Here the arrows point towards a species precursor.

CH2OO	0.992000
CH2OOE	0.001670
CH2OOF	0.001660
CH2OOG	0.001660
CH2OOA	0.001660
CH2OOC	0.001640
CH2OOB	0.001640
C5H8	0.000016
MACR	0.000016
C2H4	0.000007
HMACR	0.000007
ISOP34NO3	0.000005

Table 1.7: A reversed graph Page Rank test with CH_2OOE, small constent values have been removed.

Next, a test using α pinene with a bit more chemistry is done.

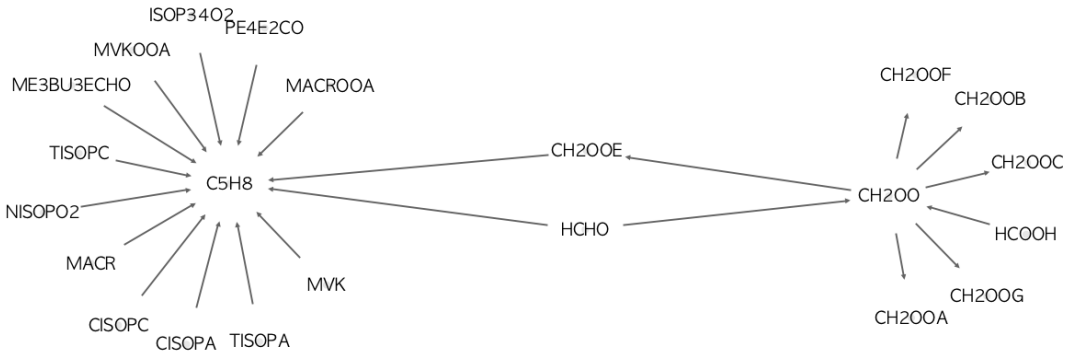

Figure 1.37: **The reversed subgraph between α-pinene, and $NC_{101}CO$** This is a subgraph of the afforementioned species, showing them and their neighbours. Here the arrows point towards a species precursor.

NC101CO	9.920000e-01
APINENE	9.210000e-06
NAPINBO	4.540000e-03
NAPINBO2	2.770000e-03
NAPINBOOH	2.690000e-03
C511OOH	-9.990000e-07
C527NO3	-9.990000e-07

Table 1.8: A reversed graph Page Rank test with $NC_{101}CO$

1.7.2 Source Analysis using the Jacobian

A bit about the maths, and procedure. This method is much easier and provides more concrete results.

1.7.3 Verdict

As the PageRank algorithm is applied to the whole network and contains teleportation it provides small values for species without a direct link to the species in question. This requires some sort of changepoint analysis to filter. A much simpler method would be the calculation of the shortest simple path between a species in question and all other species, and then subtract the value obtained within each step to get its contribution. for the example A $\xrightarrow{4}$ B $\xrightarrow{6}$ C the shortest path from A to C would be 10 and B to c would be 6. The influence of A on C would be the influence of A on B divided by the total influence on B.

The simplest is to calculate the fraction of A which contributes to B and then multiply the what B contributes to C by that fraction using the jacobian.

This section to be finished when it is not 5 am in the morning.

1.8 Conclusions

For large complex graphs, visual analytics may not form a suitable solution. Instead, it is possible to apply a range of mathematical algorithms to tell us what species are important within a network. Chemical mechanisms, much like many real-world graphs, were shown to have both small world and scale-free properties within their structure. This means that they have both a local(social) and global(hierarchical) structure.

It was shown that it is possible to generate a citation network for papers citing the master chemical mechanism and represent this in the form of a graph. Further exploration into the network structure led to the creation of a co-citation and an author network from the original dataset. This was then used to evaluate several centrality metrics, and their ability to highlight roles within the co-authorship network.

Next, the centrality metrics were applied to a range of chemical mechanisms representing urban, terrestrial and marine environments. Here it was seen that the sum of these follows a similar trend to more traditional methods of evaluating node importance, such as flux and concentration analysis. As this was the case, averaged metric values for each scenario were generated, and the individual chemistry compared with the aid of a TF-IDF algorithm. This highlights important species for each run, whilst ignoring those which are important across all runs.

Finally, it was noted that in reversing the direction of links within a graph it is possible to determine the source of influence on a node. An attempt to do this using the PageRank algorithm was made, although this proved to not be the most effective method to accomplish this. Instead, it was far

simpler to make use of the adjacency matrix (jacobian) and apply the transformation there to get the required results.

In this chapter the merit of using centrality metrics to mathematically analyse a complex network was shown. It is suggested that these are used in conjunction with more traditional methods of simulation evaluation to allow for a greater understanding of the roles each species have within a certain environment.

Bibliography

(2019). Lapack — Linear Algebra Package. `http://www.netlib.org/lapack/`. http://www.netlib.org/lapack/.

Barabási, A.-L. (2019). Nature-150-Cover.Pdf. *Nature*, 575(7781). Accessed 20-01-2020.

Bastian, M., Heymann, S., and Jacomy, M. (2009). Gephi: An open source software for exploring and manipulating networks. *AAAI*. http://www.aaai.org/ocs/index.php/ICWSM/09/paper/view/154.

Beel, J., Gipp, B., Langer, S., and Breitinger, C. (2016). Research-paper recommender systems: A literature survey. *International Journal on Digital Libraries*, 17(4):305–338.

Bloss, C., Wagner, V., Jenkin, M. E., Volkamer, R., Bloss, W. J., Lee, J. D., Heard, D. E., Wirtz, K., Martin-Reviejo, M., Rea, G., Wenger, J. C., and Pilling, M. J. (2005). Development of a detailed chemical mechanism (mcmv3.1) for the atmospheric oxidation of aromatic hydrocarbons. *Atmospheric Chemistry and Physics*, 5(3):641–664.

Bloss, W. J., Lee, J. D., Bloss, C., Heard, D. E., Pilling, M. J., Wirtz, K., Martin-Reviejo, M., and Siese, M. (2004). Validation of the calibration of a laser-induced fluorescence instrument for the measurement of oh radicals in the atmosphere. *Atmospheric Chemistry and Physics*, 4(2):571–583.

Bonacich, P. (1987). Power and centrality: A family of measures. *American Journal of Sociology*, 92(5):1170–1182. http://www.jstor.org/stable/2780000.

Bonacich, P. (2007). Some unique properties of eigenvector centrality. *Social Networks*, 29(4):555 – 564.

Borgatti, S. P. (2005). Centrality And Network Flow. *Social networks*, 27(1):55–71.

Boudin, F. (2013). A Comparison Of Centrality Measures For Graph-Based Keyphrase Extraction.

Brandes, U. (2001). A faster algorithm for betweenness centrality. *Journal of Mathematical Sociology*, 25:163–177.

Brasseur, G. and Jacob, D. (2017). *Modeling Of Atmospheric Chemistry*. Cambridge University Press.

Broido, A. D. and Clauset, A. (2019). Scale-Free Networks Are Rare. *Nature communications*, 10(1):1017.

Cabello, R. (2019). Three.Js – Javascript 3D Library. `https://threejs.org/`. Accessed: 2020-1-25.

Cajal, S. R. (2020). Cortex drawings. *web*. Accessed: 2020-2-4.

Clauset, A., Shalizi, C. R., and Newman, M. E. J. (2009). Power-Law Distributions In Empirical Data. *SIAM Review*, 51(4):661–703.

Cornell, L. (2020). Mark 1 Perceptron. `https://en.wikipedia.org/w/index.php?title=Perceptron&oldid=935763442`. Accessed: 2020-2-4.

de Solla Price, D. J. (1965). Networks of scientific papers. *Science*, 149(3683):510–515.

Derwent, R. G., Jenkin, M. E., Saunders, S. M., and Pilling, M. J. (1998). Photochemical Ozone Creation Potentials For Organic Compounds In Northwest Europe Calculated With A Master Chemical Mechanism. *Atmospheric environment*, 32(14):2429–2441.

Dillon, T. J., Tucceri, M. E., and Crowley, J. N. (2006). Laser induced fluorescence studies of iodine oxide chemistry part ii. the reactions of io with ch3o2, cf3o2 and o3. *Phys. Chem. Chem. Phys.*, 8:5185–5198.

Ebel, H., Mielsch, L.-I., and Bornholdt, S. (2002). Scale-free topology of e-mail networks. *Phys. Rev. E*, 66:035103.

Edsu and Ellis, D. (2019). Etudier. https://github.com/wolfiex/etudier.

Ellis, D. (2019). Using Tf-Idf To Form Descriptive Chapter Summaries Via Keyword Extraction. `https://towardsdatascience.com/using-tf-idf-to-form-descriptive-chapter-summaries-via-keyword-extraction-4e6fd857d190`. Accessed: 2020-2-5.

Elshorbany, Y. F., Kleffmann, J., Hofzumahaus, A., Kurtenbach, R., Wiesen, P., Brauers, T., Bohn, B., Dorn, H.-P., Fuchs, H., Holland, F., Rohrer, F., Tillmann, R., Wegener, R., Wahner, A., Kanaya, Y., Yoshino, A., Nishida, S., Kajii, Y., Martinez, M., Kubistin, D., Harder, H., Lelieveld, J., Elste, T., Plass-Dülmer, C., Stange, G., Berresheim, H., and Schurath, U. (2012). Ho X Budgets During Hoxcomp: A Case Study Of Ho X Chemistry Under No X -Limited Conditions. *Journal of geophysical research*, 117(D3).

Fantin, V., Buttol, P., Pergreffi, R., and Masoni, P. (2012). Life Cycle Assessment Of Italian High Quality Milk Production. A Comparison With An Epd Study. *Journal of cleaner production*, 28:150–159. http://www.sciencedirect.com/science/article/pii/S095965261100388X.

Freeman, L. (1977). A set of measures of centrality based on betweenness. 40:35–41.

Freeman, L., Borgatti, S., and White, D. (1991). Centrality in valued graphs: A measure of betweenness based on network flow. *Social Networks*, 13:141–154.

Freeman, L. C. (1978). Centrality in social networks conceptual clarification. *Social networks*, 1(3):215–239.

Fujita, M., Inoue, H., and Terano, T. (2017). Searching promising researchers through network centrality measures of co-author networks of technical papers. In *2017 IEEE 41st Annual Computer Software and Applications Conference (COMPSAC)*, volume 2, pages 615–618.

Gemma, J. (2019). The Most Influential Men And Women On Twitter 2017. `https://www.brandwatch.com/blog/react-influential-men-and-women-2017/`. Accessed: 2019-4-28.

Géron, A. (2017). *Hands-On Machine Learning With Scikit-Learn And Tensorflow: Concepts, Tools, And Techniques To Build Intelligent Systems*. O'Reilly Media.

Goh, K. I., Kahng, B., and Kim, D. (2001). Universal Behavior Of Load Distribution In Scale-Free Networks. *Physical review letters*, 87(27 Pt 1):278701.

Google (2019). Google Scholar. `https://scholar.google.com/schhp?hl=en`. Accessed: 2020-1-25.

Hagberg, A. A., Schult, D. A., and Swart, P. J. (2008). Exploring network structure, dynamics, and function using networkx. In Varoquaux, G., Vaught, T., and Millman, J., editors, *Proceedings of the 7th Python in Science Conference*, pages 11 – 15, Pasadena, CA USA.

Hobson, E. A., Mønster, D., and DeDeo, S. (2018). Strategic Heuristics Underlie Animal Dominance Hierarchies And Provide Evidence Of Group-Level Social Knowledge.

Humphries, M. D. and Gurney, K. (2008). Network 'Small-World-Ness': A Quantitative Method For Determining Canonical Network Equivalence. *PloS one*, 3(4):e0002051.

Jacob, P.-M. and Lapkin, A. (2018). Statistics of the network of organic chemistry. *React. Chem. Eng.*, 3:102–118. http://dx.doi.org/10.1039/C7RE00129K.

Jeanningros, Y., Vlaeminck, S. E., Kaldate, A., Verstraete, W., and Graveleau, L. (2010). Fast Start-Up Of A Pilot-Scale Deammonification Sequencing Batch Reactor From An Activated Sludge Inoculum. *Water science and technology: a journal of the International Association on Water Pollution Research*, 61(6):1393–1400. http://dx.doi.org/10.2166/wst.2010.019.

Jenkin, M. E. and Hayman, G. D. (1999). Photochemical Ozone Creation Potentials For Oxygenated Volatile Organic Compounds: Sensitivity To Variations In Kinetic And Mechanistic Parameters. *Atmospheric environment*, 33(8):1275–1293.

Jenkin, M. E., Saunders, S. M., and Pilling, M. J. (1997). The tropospheric degradation of volatile organic compounds: A protocol for mechanism development. *Atmospheric Environment*, 31(1):81 – 104.

Jenkin, M. E., Saunders, S. M., Wagner, V., and Pilling, M. J. (2003). Protocol for the development of the master chemical mechanism, mcm v3 (part b): Tropospheric degradation of aromatic volatile organic compounds. *Atmospheric Chemistry and Physics*, 3(1):181–193.

Jenkin, M. E., Young, J. C., and Rickard, A. R. (2015). The mcm v3.3.1 degradation scheme for isoprene. *Atmospheric Chemistry and Physics*, 15(20):11433–11459.

John Hay, Ben Lynch, D. S. (1960). Mark 1 Perceptron Operators' Manual. *Cornell Aeronautical Laboratory*.

Jones, E., Oliphant, T., Peterson, P., et al. (2001–). Scipy: Open source scientific tools for Python. http://www.scipy.org/.

Kleinberg, J. M. (1999). Authoritative Sources In A Hyperlinked Environment. *Journal of the ACM*, 46(5):604–632.

Korke, R., Gatti, M. d. L., Lau, A. L. Y., Lim, J. W. E., Seow, T. K., Chung, M. C. M., and Hu, W.-S. (2004). Large Scale Gene Expression Profiling Of Metabolic Shift Of Mammalian Cells In Culture. *Journal of biotechnology*, 107(1):1–17.

Krebs, V. E. (2002). Mapping Networks Of Terrorist Cells. *Connections*, 24(3):43–52.

Kumar, R. and Upfal, E. (2000). The Web As A Graph.

Langville, A. and Meyer, C. (2005). A Survey Of Eigenvector Methods For Web Information Retrieval. *SIAM Review*, 47(1):135–161.

Ling, Z. H., Guo, H., Lam, S. H. M., Saunders, S. M., and Wang, T. (2014). Atmospheric photochemical reactivity and ozone production at two sites in hong kong: Application of a master chemical mechanism–photochemical box model. *Journal of Geophysical Research: Atmospheres*, 119(17):10567–10582.

McCulloch, W. S. and Pitts, W. (1943). A logical calculus of the ideas immanent in nervous activity. *The bulletin of mathematical biophysics*, 5(4):115–133.

Mohanty, J. G., Nagababu, E., and Rifkind, J. M. (2014). Red Blood Cell Oxidative Stress Impairs Oxygen Delivery And Induces Red Blood Cell Aging. *Frontiers in physiology*, 5:84. http://dx.doi.org/10.3389/fphys.2014.00084.

Molontay, R. and Nagy, M. (2020). Twenty Years Of Network Science: A Bibliographic And Co-Authorship Network Analysis. *arXiv*.

Monastersky, R. and Van Noorden, R. (2019). 150 Years Of Nature: A Data Graphic Charts Our Evolution. *Nature*, 575(7781):22–23.

Mquantin (2020). Idf response functions. *wikipedia commons*. Accessed: 2020-2-5.

Needham, M. and Hodler, A. E. (2019). Practical Examples In Apache Spark & Neo4J. *O'Reilly*.

Newman, M. E. J. (2004). Coauthorship networks and patterns of scientific collaboration. *Proceedings of the National Academy of Sciences*, 101(suppl 1):5200–5205.

Oliphant, T. (2006). Guide to numpy.

Ottens, A. K., Kobeissy, F. H., Golden, E. C., Zhang, Z., Haskins, W. E., Chen, S.-S., Hayes, R. L., Wang, K. K. W., and Denslow, N. D. (2006). Neuroproteomics In Neurotrauma. *Mass spectrometry reviews*, 25(3):380–408. http://dx.doi.org/10.1002/mas.20073.

Page, L., Brin, S., Motwani, R., and Winograd, T. (1999). The pagerank citation ranking: Bringing order to the web. *Stanford InfoLab*, (1999-66). Previous number = SIDL-WP-1999-0120 `http://ilpubs.stanford.edu:8090/422/`.

Pokroy, B., Epstein, A. K., Persson-Gulda, M. C. M., and Aizenberg, J. (2009). Fabrication Of Bioinspired Actuated Nanostructures With Arbitrary Geometry And Stiffness. *Advanced materials*, 21(4):463–469. http://doi.wiley.com/10.1002/adma.200801432.

poliaktiv (2011). Social Network Analysis: Theory And Applications.

Press, W. H., Teukolsky, S. A., Vetterling, W. T., and Flannery, B. P. (1992). *Numerical Recipes In C (2Nd Ed.): The Art Of Scientific Computing*. Cambridge University Press, USA.

R. Seeley, J. (1949). The net of reciprocal influence: A problem in treating sociometric data. *Canadian Journal of Psychology/Revue canadienne de psychologie*, 3:234–240.

Rosenblatt, F. (1958). The perceptron: A probabilistic model for information storage and organization in the brain. *Psychological Review*, pages 65–386.

Sabidussi, G. (1966). The centrality index of a graph. *Psychometrika*, 31(4):581–603.

Saunders, S. M., Jenkin, M. E., Derwent, R. G., and Pilling, M. J. (2003). Protocol For The Development Of The Master Chemical Mechanism, Mcm V3 (Part A): Tropospheric Degradation Of Non-Aromatic Volatile Organic Compounds. *Atmospheric Chemistry and Physics*, 3(1):161–180.

Small, H. (1973). Co-citation in the scientific literature: A new measure of the relationship between two documents. *Journal of the American Society for Information Science*, 24(4):265–269.

Spencer, R. G. M., Hernes, P. J., Ruf, R., Baker, A., Dyda, R. Y., Stubbins, A., and Six, J. (2010). Temporal Controls On Dissolved Organic Matter And Lignin Biogeochemistry In A Pristine Tropical River, Democratic Republic Of Congo. *Journal of geophysical research*, 115(G3):2069. http://doi.wiley.com/10.1029/2009JG001180.

Stubbins, A., Hubbard, V., Uher, G., Law, C. S., Upstill-Goddard, R. C., Aiken, G. R., and Mopper, K. (2008). Relating Carbon Monoxide Photoproduction To Dissolved Organic Matter Functionality. *Environmental science & technology*, 42(9):3271–3276.

Turányi, T. and Tomlin, A. S. (2014). *Reduction Of Reaction Mechanisms*. Springer Berlin Heidelberg, Berlin, Heidelberg.

Vigna, S. (2016). Spectral Ranking. *Network Science*, 4(4):433–445.

Watts, D. J. and Strogatz, S. H. (1998). Collective Dynamics Of 'Small-World' Networks. *Nature*, 393(6684):440–442.

Wood, B. (2014). The Origin Of Humans Is Surprisingly Complicated. *Scientific American*. `https://www.scientificamerican.com/article/the-origin-of-humans-is-surprisingly-complicated/`.